Journal of Molecular and Cellular Cardiology 134 (2019) 13–28

Contents lists available at ScienceDirect

Journal of Molecular and Cellular Cardiology

journal homepage: www.elsevier.com/locate/yjmcc

Inhibition of Rho-associated kinases suppresses cardiac myofibroblast function in engineered connective and heart muscle tissues

Gabriela Leão Santos[a,b,d], Svenja Hartmann[a,b,d], Wolfram-Hubertus Zimmermann[a,d], Anne Ridley[b,c], Susanne Lutz[a,d,*]

[a] Institute of Pharmacology and Toxicology, University Medical Center Göttingen, Germany
[b] Randall Centre for Cell and Molecular Biophysics, King's College London, London, UK
[c] School of Cellular and Molecular Medicine, University of Bristol, UK
[d] DZHK (German Center for Cardiovascular Research) Partner Site, Göttingen, Germany

A B S T R A C T

Cardiac fibrosis is a hallmark of heart failure for which there is no effective pharmacological therapy. By genetic modification and in vivo inhibitor approaches it was suggested that the Rho-associated kinases (ROCK1 and ROCK2) are involved in pro-fibrotic signalling in cardiac fibroblasts and that they may serve as targets for anti-fibrotic therapies. We demonstrate that simultaneous inhibition of ROCK1 and ROCK2 strongly interfered with tissue formation and their biomechanical properties in a model of engineered connective tissue (ECT), comprised of cardiac fibroblasts and collagen. These effects were observed with both rat and human ECT. Inhibitors of different chemistries, including the isoquinoline inhibitors Fasudil and H1152P as well as the pyrazol-phenyl inhibitor SR-3677, showed comparable effects. By combined treatment of ECT with TGF-β and H1152P, we could identify ROCK as a mediator of TGF-β-dependent tissue stiffening. Moreover, expression analyses suggested that lysyl oxidase (LOX) is a downstream target of the ROCK-actin-MRTF/SRF pathway and inhibition of this pathway by Latrunculin A and CCG-203971 showed similar anti-fibrotic effects in the ECT model as ROCK inhibitors. In line with the collagen crosslinking function of LOX, its inhibition by β-aminopropionitrile resulted in reduced ECT stiffness, but let tissue compaction unaffected. Finally, we show that ROCK inhibition also reduced the compaction and stiffness of engineered heart muscle tissues. Our results indicate that pharmacological inhibition of ROCK has a strong anti-fibrotic potential which is in part due to a decrease in the expression of the collagen crosslinking enzyme lysyl oxidase.

1. Introduction

Cardiac fibrosis is a self-perpetuating process, which takes place in the diseased heart. The increase in interstitial and perivascular extracellular matrix accumulation leads to diastolic dysfunction, diffusion problems, cardiomyocyte death and arrhythmias. Therapeutically, blockade of the renin-angiotensin II (Ang II)-aldosterone system by angiotensin converting enzyme (ACE) inhibitors or angiotensin II-type1 receptor antagonists can slow down fibrosis [1], but it is not yet possible to halt or reverse fibrosis. Cardiac fibrosis is driven by myofibroblasts, which arise mainly from transdifferentiation of resident cardiac fibroblasts after exposure to mediators like Ang II and transforming growth factor-β as well as in response to altered biomechanical properties of their surroundings [2–5]. Understanding the molecular events underlying fibrosis is essential to identify new therapeutic anti-fibrotic strategies for the treatment of heart failure.

The RhoA-associated kinases ROCK1 and ROCK2 are serine/threonine kinases belonging to the family of AGC-kinases. Both have been suggested to play a role in cardiac disease and in remodelling of the myocardium [6]. Studies using ROCK1 and ROCK2-deficient mice indicate that ROCKs regulate cardiomyocyte apoptosis and cardiac fibrosis [7–12]. In addition, ROCK2 was shown to contribute to cardiac hypertrophy [8,11]. In vitro, ROCKs regulate fibrosis-associated genes, including connective tissue growth factor (CTGF), fibroblast growth factor 2 (FGF2), α-smooth muscle actin (SMA) and pro-collagen I [10,13–15]. ROCKs are also implicated in cardiac fibroblast migration and proliferation [16–18]. All in vitro studies have been carried out using purified cardiac fibroblasts in 2D cultures, and the effects of ROCK inhibition on the behaviour of cardiac fibroblasts embedded in a more physiological 3D environment have not been investigated.

Tissue engineering approaches are improving our understanding of cellular processes taking place in a 3D environment, as well as facilitating the discovery of druggable targets using drug screening. The idea of using engineered connective tissues to study fibrotic processes was brought up in the late 80s of the last century [19]. In the following these tissues were mainly used to understand the biology of embedded fibroblasts and to learn more about their influence on biomechanical tissue properties [20]. A further development of these tissues led to the nowadays widely used heterogeneous cardiac tissues consisting of matrix factors, cardiomyocytes and non-cardiomyocytes [21–23].

* Corresponding author at: Institute of Pharmacology and Toxicology, University Medical Center Göttingen, Robert-Koch Str. 40, 37075 Göttingen, Germany.
E-mail address: Susanne.Lutz@med.uni-goettingen.de (S. Lutz).

https://doi.org/10.1016/j.yjmcc.2019.06.015
Received 5 December 2018; Received in revised form 1 June 2019
Available online 22 June 2019

Unfortunately, homogeneous cardiac fibroblast tissues has received less attention, although they could serve as simple test beds to specifically address cardiac fibrosis mechanisms. We introduced a ring-shaped engineered connective tissue (ECT) model composed of cardiac fibroblasts and collagen I, which offers several advantages compared to other models like floating discs, aggregates with or without collagen, and sheet-like tissues [24–28]. In the ring-shaped model, the cells compress the matrix against a central stiff rod, which does not allow them to contract the tissue into an undefined ball-like structure. This enables the simple quantification of tissue compaction by measuring the cross sectional area of the tissues. Moreover, the stiff rod applies a moderate tension to the cells, which can induce the alignment of fibroblasts along the tension axis mimicking the natural situation [29]. The ring-shape minimizes in addition non-uniformity in tissue geometry and environmental differences affecting the embedded cells [29]. And most importantly, the ring-shape enabled us to measure the biomechanical properties with hooks and a rheometer without damaging the tissue by clamps or similar. We perform linear ultimate destructive tensile measurements in order to obtain information on tissue stiffness (Young's modulus, slope of the elastic region of the stress-strain curve) and on the strain to failure point reflecting the maximal extensibility of the tissue. We have previously demonstrated that this model is suitable to perform gain and loss of function experiments as well as small molecule studies [15,18,30].

Here, we introduce a two-tiered approach to identify anti-fibrotic targets in a homogeneous rat and human cardiac fibroblast- (rECT and hECT) and heterogeneous rat cardiac cell- (rEHM) specific context. Both models allow for direct and quantitative assessments of fibroblasts on viscoelastic properties and in case of rEHM an association to contractile function. By making use of 2D, rECT, hECT and rEHM models we identified that ROCK inhibition results in a substantial loss of tissue compaction and a decline in tissue stiffness. We further observed that ROCK inhibition blunts the TGF-β-dependent increase of tissue stiffness and that tissue stiffening involves a ROCK-mediated regulation of the collagen cross-linking enzyme lysyl oxidase (LOX).

2. Material and methods

2.1. Material

All cell culture reagents for the growth of rat cardiac cells were purchased from Invitrogen, unless otherwise stated. Cell culture plastic was obtained from Greiner, Sarstedt or Nunc. All fine chemicals were of highest quality available and were purchased from Sigma Aldrich (DAPI, FITC-phalloidin, Hoechst 33342, β-aminopropionitrile, CCG-203971), Biomol (Fasudil, H1152P, SR-3677), Preprotech (TGF-β), Enzo Life Sciences (Latrunculin A) or Merck (MMP 408). Antibodies were purchased from BD Biosciences (ROCK1, 611,136), Santa Cruz (ROCK2, sc-5561), Origene (LOX, TA337077), Zytomed Systems (GAPDH, RGM2-6C5) and Sigma Aldrich (α-tubulin, T 5168; β-actin, A 2228; α-smooth muscle Actin (SMA), A 5228). All primers were synthesized by Eurofins Genomics.

2.2. Animal care and housing

Animals were used in accordance with the guidelines (§4 Absatz 3 Deutsches Tierschutzgesetz) of the institutional animal care and use committee Niedersächsisches Landesamtes für Verbraucherschutz und Lebensmittelsicherheit (LAVES, Germany). Rats were kept on a 12 h light/dark cycle with water and food ad libitum.

2.3. Isolation of neonatal rat cardiac cells

Neonatal rat cardiac fibroblasts (NRCF) and cardiomyocytes (NRCM) were isolated using the neonatal heart dissociation kit, mouse and rat from Miltenyi Biotec. Forty to sixty neonatal Wistar rats (P0-P3) were decapitated, a thoracotomy performed, and the heart including the vascular pedicle was excised. The atria, vascular pedicle and remaining connective tissue were dissected. The tissue was digested according to the manufacturer's instructions and dispersed with the gentleMACS dissociator (Miltenyi Biotec) using the gentleMACS program htumor3.01. Cells were then resuspended in NCM medium (DMEM GlutaMAX 1 g/L glucose, 10% fetal calf serum (v/v) 1% penicillin-streptomycin (v/v)) and strained through a 250 μm pore stainless steel mesh. The cell suspension was centrifuged, the supernatant was discarded, and the pellet resuspended in NCM medium. This cell mixture was either directly used to prepare engineered heart muscle tissues (EHM) or further processed to purify the fraction of cardiac fibroblasts. To obtain fibroblasts, 8×10^6 cardiac cells were seeded on a 15 cm cell culture dish in NCM medium and incubated for 45 min in a humidified incubator (37 °C, 5% CO_2). The unattached cardiomyocytes were removed with several washing steps. The attached NRCF were cultivated in NRCF growth medium (DMEM GlutaMAX 4.5 g/L glucose, 10% fetal calf serum (v/v), 1% penicillin-streptomycin (v/v) 1% non-essential amino acids (v/v)). For experiments NRCF from passage 2 to 3 were used.

2.4. Cultivation of normal human ventricular cardiac fibroblasts

Normal human ventricular cardiac fibroblasts (hCF) were purchased from Lonza. The cells had been isolated from a male Caucasian donor. They were cultivated in FGM-3 growth medium (Lonza) according to the manufacturer's recommendations. For the preparation of hECT, cell passages 3 to 4 were used.

2.5. Inhibitor treatments

Dilution of H1152P was carried out in DMSO. We therefore added DMSO in an equal volume to all conditions including the controls to avoid DMSO effects.

2.6. Proliferation assay

The proliferation of NRCF was analysed over six days. In a 24-well plate 10^4 NRCF were seeded per well in NRCF growth medium and treated with 300 nM or 3 μM H1152P every day starting 24 h after seeding. The cells were fixed with 4% paraformaldehyde (PFA) in PBS for 15 min 24 h after seeding and 1, 2, and 6 days later. The cell nuclei were stained with 10 μg/mL Hoechst 33342 in PBS for 30 min. Automated evaluation of cell number was performed using the Cellavista system (Synentec).

2.7. Adhesion assay

NRCF were treated for 24 h with 300 nM or 3 μM H1152P, or left untreated. The cells were then replated in NRCF growth medium containing the ROCK inhibitors on uncoated or collagen type I-coated (50 μg/cm^2) 12-well plates. After 20, 40 and 60 min ten bright-field images per condition were acquired using the time-lapse function of an inverted microscope (Olympus) equipped with a XM10 camera (Olympus), 10× objective and a humidified climate chamber set to 37 °C, 5% CO_2. The number of adhered cell and all cells were manually counted.

2.8. Apoptosis assay

NRCF were pre-conditioned for 24 h with reduced serum (2%)-containing NRCF medium and treated with 300 nM or 3 μM H1152P for 48 h. As a positive control, cells were treated with 3 μM staurosporine for 3 h. Upon treatment, cells were washed twice with PBS and stained with FITC-conjugated annexin-V and propidium iodide (PI) according to the manufacturer's instructions (Annexin-V-FLUOS Staining Kit,

Roche). The stained cells were imaged under an Olympus IX81 inverted fluorescence microscope.

2.9. Analysis of the actin cytoskeleton, bi-nucleation and cell area of NRCF in 2D cultures

NRCF were cultured in NRCF growth medium in the presence of 300 nM or 3 μM H1152P. After 48 h the cells were washed with PBS and fixed with 4% paraformaldehyde in PBS for 15 min. After three PBS washing steps permeabilization was carried out in 0.02% Triton X-100 in PBS for 3 min. Staining of the actin cytoskeleton with 0.5 μg/mL FRITC-labelled phalloidin and of the nuclei with 1 μg/mL DAPI in PBS was performed for 1 h at room temperature in the dark. Finally, the cells were washed twice with PBS and imaged using an inverted fluorescence microscope (Olympus) with a XM10 camera (Olympus) and a 10× objective. Bi-nucleated cells were counted and cell size analysis was performed with the free hand tool of ImageJ.

2.10. Preparation and cultivation of rat engineered connective tissues (rECT)

To generate rECT, 1.2 mg rat tail collagen type I (purified in-house or obtained from Corning) was neutralized with 0.1 N NaOH, buffered with 2× DMEM (20% 10× DMEM (*v*/v), 20% horse serum (v/v) 2% penicillin-streptomycin (v/v)) and then mixed with 1.7×10^6 NRCF per tissue. The mixture was cast into custom-made circular moulds (diameter of the inner spacer 8 mm) and allowed to gel for 1 h in a humidified incubator at 37 °C and 5% CO_2. After condensation, NRCF growth medium was added to the casting mould and the tissues were cultured for 5 days without further treatment or as indicated in the presence of 10 μM Fasudil, 3 μM H1152P, 3–170 nM SR-3677, 100 μM β-aminopropionitrile (BAPN), 5 ng/mL TGF-β1, 7 ng/mL LatA, 50 μM CCG-203971 and/or 10 μM MMP408. The reagent-containing as well as the control media were changed every day. rECT from different experiment.

2.11. Preparation and cultivation of human engineered connective tissues (hECT)

To generate hECT, 0.6 mg bovine collagen type I (Collagen solutions LLC) was neutralized with 0.1 N NaOH, buffered with 2× DMEM and then mixed with 0.75×10^6 hCF per tissue. The mixture was cast into custom-made circular moulds and allowed to gel for 1 h in a humidified incubator at 37 °C and 5% CO_2. The used moulds were half the size (diameter of the inner spacer 4 mm) of those used for rECT preparation. After condensation, FGM-3 growth medium was added to the casting mould and the tissues were cultured for 5 days without further treatment or as indicated in the presence of 10 μM Fasudil or 3 μM H1152P. The inhibitor-containing medium was changed every day.

2.12. Preparation and cultivation of rat engineered heart muscle tissues (rEHM)

EHM were generated as described before [31]. In brief, 0.8 mg rat tail collagen type I (purified in-house) was neutralized with 0.1 N NaOH, buffered with 2× DMEM and mixed with 10% Matrigel (Corning) and 2.5×10^6 isolated rat cardiac cells per tissue. The rEHMs were cast into custom-made circular moulds (diameter of the inner spacer 8 mm) and allowed to solidify for 1 h in a humidified incubator at 37 °C and 5% CO_2. After gelation, rEHM culture medium (DMEM GlutaMAX, 1 g/L glucose, 10% horse serum (*v*/v), 1% penicillin-streptomycin (v/v)) was added to the casting mould. The medium was changed the next day and then every second day thereafter. On culture day eight, the rEHMs were subjected to dynamic mechanical stretch at 1 Hz for 24 h, then at 2 Hz for another six days. During this phase, the rEHMs were treated with 10 μM Fasudil or 3 μM H1152P. The medium was changed every other day.

2.13. Cross-sectional area analysis of engineered tissues

The engineered tissues were taken out of their casting moulds (ECT) or were removed from the phasic stretchers (rEHM), transferred in a multi-well plate and imaged with a stereomicroscope (Stereo Lumar.V12, Zeiss). Images of the tissues were taken from top and from the side. Horizontal line scan analysis was performed at a minimum of 3 positions per tissue arm per image. The cross-sectional area (CSA) was calculated based on the means of the line lengths, which approximately reflect the tissues' diameters (mean diameter top d_t, mean diameter side d_s), with the help of the elliptic area equation $CSA = d_t/2 \times d_s/2 \times \pi$. We used the CSA in the following as a measure for differences in tissue compaction, which describes changes that occur during the gelation of collagen, the cell-driven compression of the matrix and/or the re-modelling of the matrix by secreted factors.

2.14. Destructive tensile strength of engineered tissues

Destructive tensile strength of engineered tissues was performed using an RSA-G2 rheometer (TA Instruments) to assess their viscoelastic properties. The engineered tissues were transferred into an organ bath containing PBS at 37 °C and fixed between two custom-made hooks. Tissues were then stretched at a constant linear rate of 0.05 mm/s for rat and 0.03 mm/s for human tissues until the point of rupture.

2.15. Stress-strain analysis of destructive tensile strength measurements

To calculate the given parameters (Young's modulus, strain to failure point) from the destructive tensile strength measurements, the measured force values (mN) were divided by the determined CSA (mm^2) to obtain stress values (kPa) and these were plotted against the gap in mm (distance between the upper and lower hook) in GraphPad Prism. The obtained curves typically displayed the following regions: An initial region in which only background stress was measured, a short toe region, an elastic region in which the stress versus gap values were linear, a flattened plastic region, and finally a region of failure which was characterized by a sudden drop in stress due to the rupture of the tissues. To calculate the strain values, the beginning of the toe region was identified and the corresponding gap length was considered as L_0. The strain equation $(L_{total}\text{-}L_0)/L_0$ was used to transform the gap values, and the stress values at the beginning of the toe region were used for background subtraction. The slope of the elastic region was determined by linear regression and is presented in this work as Young's modulus. The strain to failure point, characterized by the sudden drop in stress, was identified manually. Due to the material-dependent variations in the absolute values, we compared only conditions which had been tested in parallel.

2.16. Isometric force measurements of rEHM

After 14 days in culture, the rEHM functionality was assessed by isometric force measurements in an organ bath containing oxygenated Tyrode's solution at 37 °C. Prior to force measurements, the force transducers were calibrated. The rEHM were stretched by stepwise length adjustment (in 125 μm steps) at 2 Hz electrical field stimulation in the presence of 1 mM extracellular calcium until the length of maximum force generation was reached. The contractile forces of rEHM were measured in the presence of increasing extracellular calcium (0.2–2.4 mM).

2.17. Re-isolation of cells from rECT

rECT were dissociated by incubation in 2 mg/mL collagenase I in calcium-containing PBS in the presence of 20% FCS for 2 h at 37 °C. The

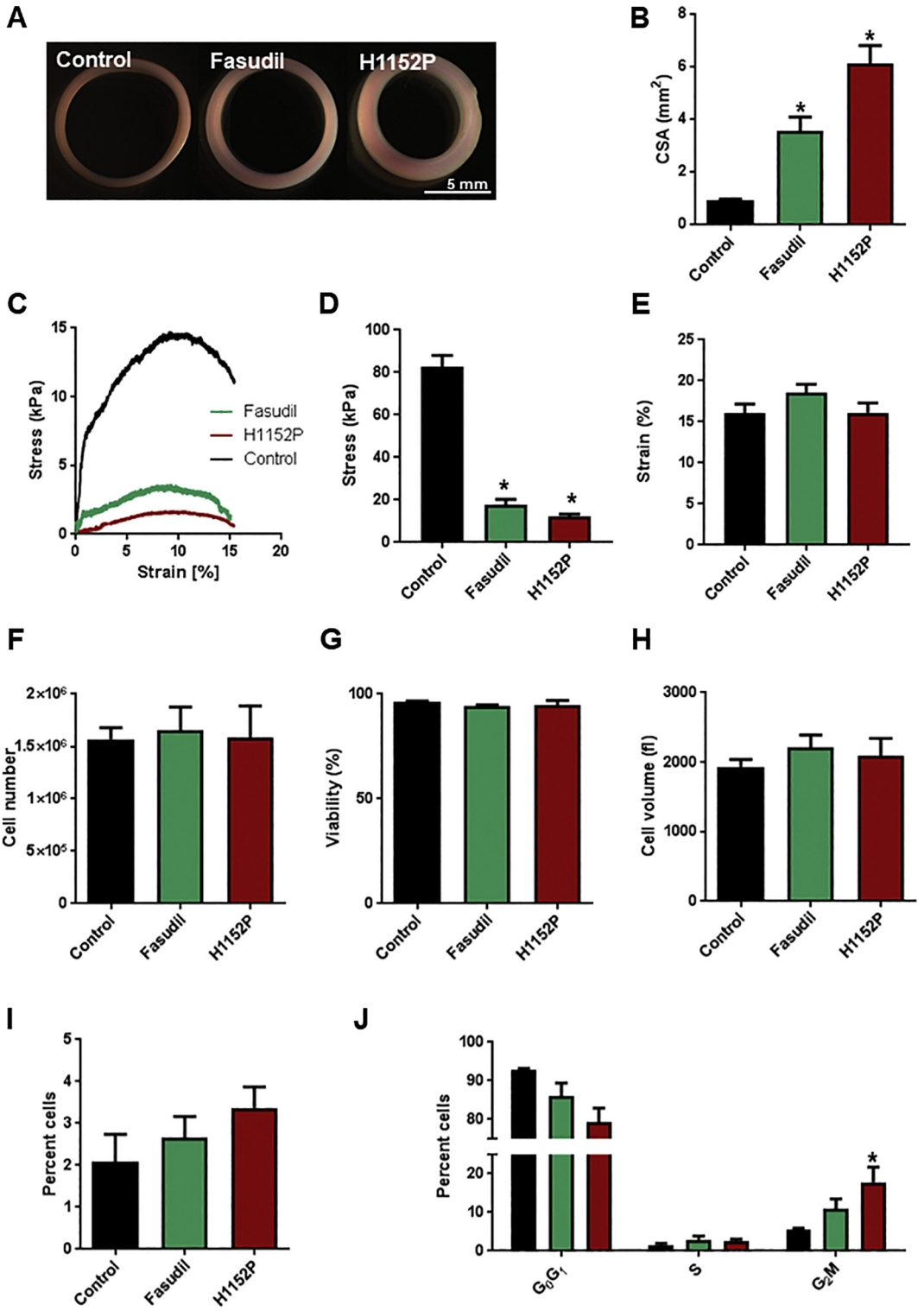

Fig. 1. ROCK inhibition reduced compaction and stiffness of rECT. rECT were generated with NRCF and collagen I and were cultured for 5 days in the absence (Control) or presence of 10 μM Fasudil or 3 μM H1152P. A) Representative images of rECT are shown. B) The cross sectional areas (CSA) were determined by image analysis. Given are the means + SEM of 13 to 15 individual tissues from 3 independent experiments. Differences were analysed by 1way-ANOVA, $*p < .05$ vs. Control. C) Representative stress-strain curves from destructive tensile measurements are shown. D) The Young's moduli were calculated based on the obtained stress-strain curves. Given are the means + SEM of 9–13 rECT from 3 independent experiments. Differences were evaluated by 1way-ANOVA, $*p < .05$ vs. Control. E) The strain to failure point was extracted from the obtained rheology data. Given are the means + SEM of 13–17 rECT from 3 independent experiments. F–H) The cells were re-isolated from the rECT and the total cell numbers (F), cell viabilities (G) and cell volumes (H) were analysed. Given are the means + SEM of 6 to 8 rECT from 3 independent experiments. I, J) The re-isolated cells were fixed and FACS analysis was performed. The percentages of bi-nucleated cells (I) and of cells in different cell cycle phases (J) were determined. Shown are the means + SEM of 4 to 6 isolations. Differences in the cell cycle stage were evaluated by 2-way-ANOVA, $*p < .05$ vs. Control.

tissues were then washed with PBS and further incubated in Accutase (Millipore), 0.0125% Trypsin, and 20 μg/mL DNAse (Calbiochem) for 30 min at 37 °C. The cells were mechanically separated and the enzymatic activity was stopped by transferring them into PBS containing 5% FBS. After centrifugation for 10 min at 100 *g* and 4 °C, cells were resuspended in PBS containing 5% FBS and counted with a CASY TT system (Roche).

2.18. FACS analysis

For FACS analysis cells isolated from rECT or cultured in 2D after detachment were used. The cells were fixed in ice-cold 75% ethanol for at least 30 min at 4 °C and then washed twice in PBS. For propidium iodide staining, the cells were subsequently treated with 100 μg/mL RNase. To stain the DNA, cells were then incubated either with 50 μg/mL propidium iodide for 30 min at 37 °C or with 10 μg/mL Hoechst 33342 for 30 min at 4 °C, centrifuged for 5 min at 300 *g* and 4 °C, resuspended in PBS and then analysed by flow cytometry. Appropriate regions and gates strategy to quantify the results were hierarchically defined as follows: (1) gating of cells based on forward scatter area (FSC-A) and sideward scatter area (SSC-A) also allowing the exclusion of cell debris, (2) gating of single cells based on DNA signal width versus FSC-A, (3) gating of cell cycle phases based on DNA signal area versus FSC-A. Cells were run on a LSRII SORP Cytometer (BD Biosciences) and analysed using Flowing software. At least 10,000 events were analysed per sample.

2.19. Immunoblot analysis

Proteins were isolated from treated 2D and 3D cultures with Cytobuster (Novagen), centrifuged and the supernatant supplemented with 4× Laemmli buffer. The cell lysates were denatured and subjected to SDS-PAGE followed by transfer onto a nitrocellulose membrane. Membranes were blocked with 1× Rotiblock (Carl Roth) for 1 h at room temperature, washed once with TBST (10 mM Tris pH 7.4, 150 mM NaCl, 0.1% Tween 20) and incubated overnight with the respective antibodies. After three washing steps with TBST, the membranes were incubated with the secondary antibodies (anti-mouse Sigma-Aldrich A9044, anti-rabbit Sigma-Aldrich A9169) for 1 h. After three final washing steps, the secondary antibodies were detected with SuperSignal West Femto Maximum Sensitivity Substrate (Thermo Scientific) using a ChemiDoc imaging system (Biorad).

2.20. qPCR analysis

RNA was isolated from ECT using a phenol-chloroform method. TriFast (1 mL, Peqlab) was added per tissue and incubated at 4 °C overnight to dissolve the collagen hydrogel. The following day, remaining pieces of tissue were mechanically dissociated by vigorous pipetting and subsequent RNA isolation was performed according to the manufacturer's protocol. To further clean up the RNA, the clean-up protocol of the RNeasy Mini Kit (Qiagen) was used. For isolation of RNA from 2D NRCF cultures, QIAshredder spin columns and the RNeasy Mini Kit (Qiagen) were used according to manufacturer's protocols. The isolated total RNA was subjected to cDNA synthesis with the help of the RevertAid first strand cDNA synthesis kit (Fermentas). Quantitative real-time PCR was performed with 5× HOT FIREPol EvaGreen qPCR Mix Plus (Solis Biodyne) in 384-well plates (Applied Biosystems) with a ViiA 7 real-time PCR system (Applied Biosystems). Primers used for amplification are given in the supplement. All values were normalized to a combination of the housekeeping genes porphobilinogen deaminase (PBGD) and β-glucuronidase (GUSB), or PBGD and hypoxanthine phosphoribosyltransferase 1 (HPRT) and calculated either by a standard curve or by the ΔΔCT equation.

3. Results

3.1. ROCK inhibition reduces compaction and stiffness of rECT

The first aim of our study was to test the influence of different pan-ROCK inhibitors on the behaviour of cardiac fibroblasts in a 3D environment. We decided to compare at first the clinically approved ROCK inhibitor Fasudil with its more potent and specific homolog H1152P [32]. We generated rECT composed of neonatal rat cardiac fibroblasts (NRCF) and rat tail collagen I and treated the tissues with Fasudil (10 μM) or H1152P (3 μM). After 5 days in culture the dimensions of rECT were analysed. Compared to untreated controls, the cross-sectional areas of the Fasudil- and H1152P-treated rECT were significantly increased and the tissues appeared to be less compact, which argues for changes in cell-driven compression of the matrix and/or its remodelling by secreted factors. (Fig. 1A, B). Next, the tissues were subjected to rheometry to assess their biomechanical properties. Representative stress-strain curves are shown in Fig. 1C. Based on these curves the Young's moduli were calculated showing that Fasudil and H1152P strongly reduced tissue stiffness (Fig. 1D). No change in tissue extensibility (strain to failure point) was detected (Fig. 1E). To exclude cell loss as a cause for the observed changes, we re-isolated the cells from the tissues. The cell yield was comparable in all groups, as well as the cell viability (Fig. 1F, G). We could further exclude a change in cell size as an explanation for our findings (Fig. 1H). By FACS analysis of re-isolated and fixed cells we found no change in the percentage of binucleated cells in the H1152P-treated rECT (Fig. 1I) and a moderate increased number of cells in G2M phase (Fig. 1J). These results demonstrate that ROCK inhibition with Fasudil or H1152P strongly interferes with the ability of cardiac fibroblasts to form compact and stiff tissues. In line with their described pharmacological profiles, the more potent and selective inhibitor H1152P elicited more prominent effects [33]. As Fasudil and H1152P share the same isoquinoline chemistry, we further carried out a concentration-response analysis for the largely uncharacterized compound SR-3677. SR-3677 possesses a pyrazol-phenyl scaffold and was described to more potently inhibit ROCK2 than ROCK1 as well as to inhibit effectively in the nanomolar range [34]. We found that at the highest concentration of 170 nM, which exceeds 3-fold the IC_{50} of ROCK1 and 50-fold the IC_{50} of ROCK2, SR-3677 showed a similar reduction in rECT compaction and in the calculated Young's modulus as H1152P (Suppl.-Fig. 1). These data together strongly support a role of ROCKs in rECT tissue compaction and stiffening and demonstrates that the rECT model is suitable for drug screening and comparison.

3.2. ECT compaction and stiffness are differentially regulated by TGF-β and ROCK

ROCK signalling had been described to be part of the non-canonical TGF-β signal pathway in cardiac fibroblasts [10]. We therefore used our rECT model to analyse the impact of ROCK inhibition on TGF-β-induced changes in rECT properties. Treatment of rECT with TGF-β did not alter tissue compaction (Fig. 2A, B), but increased tissue stiffness significantly (Fig. 2C, D). As shown in Fig. 1, ROCK inhibition with 3 μM H1152P impaired both processes. Treatment with TGF-β prevented the reduction in tissue compaction and tissue stiffness induced by H1152P (Fig. 2A–D). These results indicate that TGF-β signalling compensates for the effect of ROCK inhibition on tissue compaction, and that ROCK inhibition reduces the pro-fibrotic effect of TGF-β as demonstrated by the reduction in tissue stiffness.

3.3. ROCK inhibition reduces the transcription of secreted proteins in rECT

One possible explanation for the role of ROCKs in rECT tissue properties is that they regulate the composition of the extracellular matrix. We therefore investigated the expression of a panel of genes

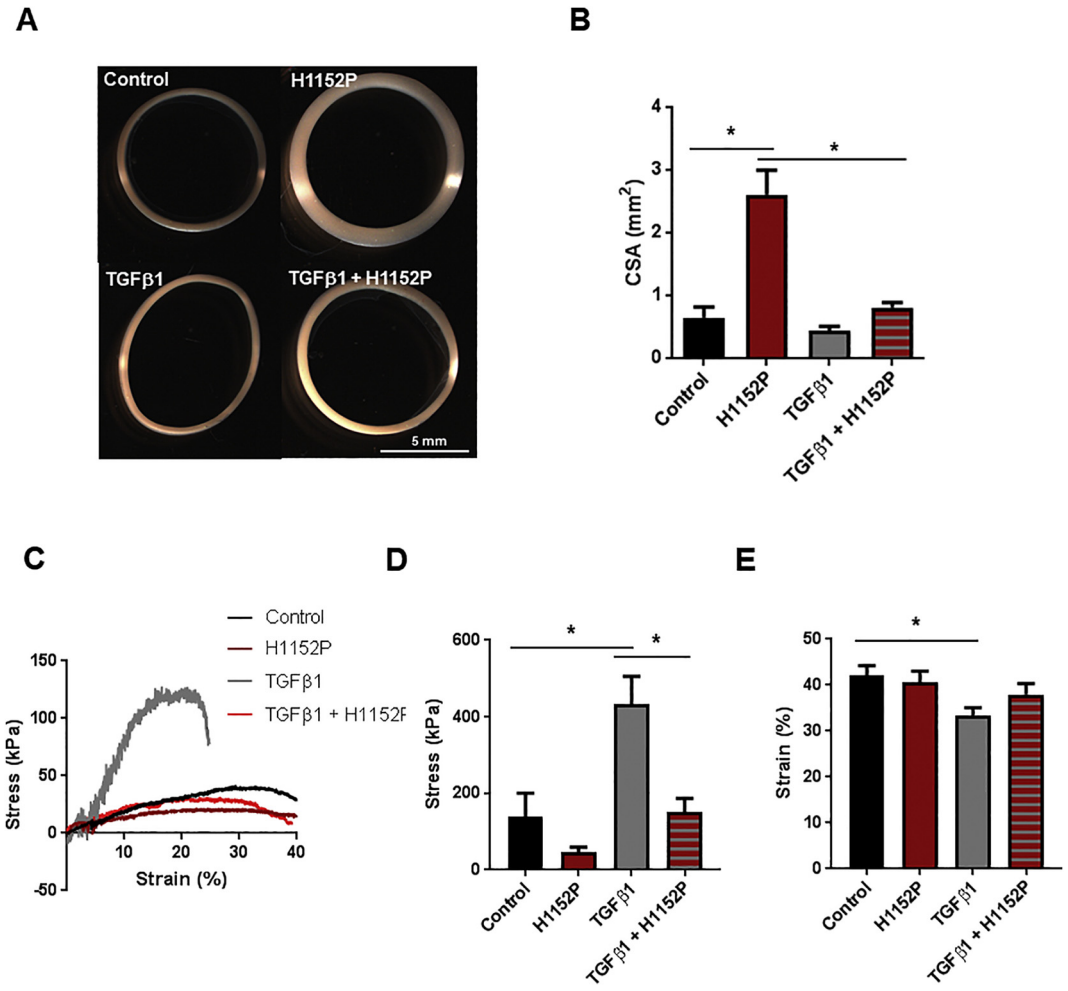

Fig. 2. rECT compaction and stiffness are differentially regulated by TGF-β and ROCK. rECT were generated with NRCF and collagen I and were cultured for 5 days in the absence (Control) or presence of 3 μM H1152P and/or 5 ng/mL TGF-β1. A) Representative images of rECT are shown. B) The cross sectional areas (CSA) were determined by image analysis. Given are the means + SEM of 3 independent experiments. Differences were analysed by 1way-ANOVA, $*p < .05$ vs. Control. C) Representative stress-strain curves from destructive tensile measurements are shown. D) The Young's moduli were calculated based on the obtained stress-strain curves. Given are the means + SEM of 3 independent experiments. Differences were evaluated by 1-way-ANOVA, $*p < .05$ vs. Control.

involved in forming, modifying or regulating the extracellular matrix, focusing particularly on those linked to collagens, since this was used to embed the cardiac fibroblasts in rECT. We extracted RNA from rECT treated with and without the ROCK inhibitors Fasudil and H1152P and performed qPCR analysis. In contrast to previous reports [10,13], we did not detect any ROCK-mediated differences in the expression of the dominant cardiac collagen isoforms collagen 1a1 (col1a1) and also not of collagen 3a1 (col3a1). Similarly, there were no differences in the expression of the collagen organizers biglycan and decorin, the fibrosis markers CTGF and galectin-3 (LGALS3) or the major pro-fibrotic cytokine TGF-β. In contrast, the transcription of the collagen crosslinker lysyl oxidase (LOX) and the fibrosis inducer hyaluronan synthase 2 (HAS2) and were decreased by Fasudil and H1152P treatment. H1152P also inhibited the transcription of the elastase MMP12 significantly. Conversely, MMP2 and ROCK2 increased following H1152P treatment (Fig. 3A). We next validated the expression changes which were consistent between Fasudil and H1152P on protein level. We performed immunoblot analyses of LOX and for control of ROCK1 and ROCK2 after 1 day and 5 days of treatment. LOX expression was reduced in ECT treated for 1 day with Fasudil and H1152P. After 5 days treatment the changes were not as prominent as after 1 day (Fig. 3B). ROCK1 was significantly increased by H1152P after 1 day (Fig. 3C), ROCK2 showed no significant changes in its protein levels at any condition (Fig. 3D). We further tried to detect HAS2, however, due to the high albumin content in our tissues we were not able to identify a reliable signal (data not shown).

3.4. ROCKs alter cardiac fibroblast cell shape, cell cycle progression and LOX expression in 2D cultures

To analyse how ROCK inhibitors affect cardiac fibroblast function, we treated NRCFs with 300 nM and 3 μM H1152P for 48 h in 2D culture conditions. H1152P appear to reduce the complexity of the intracellular actin network (Fig. 4A). The cell area was increase by H1152P, which was not based on a general increase in cell size (Fig. 4B, C). We then investigated the ability of the cells to adhere to plastic or collagen-coated surfaces as a possible explanation for the compaction defect observed in ROCK inhibitor-treated rECT, but no difference between control and H1152P-treated NRCFs was observed. As expected the adhesion to collagen-coated surfaces was in general faster than to uncoated plastic (Fig. 4D). Based on our observed cell cycle changes induced by ROCK inhibitors in rECT, we studied cell proliferation by automated counting of cell nuclei, determined the number of bi-nucleated cells and performed cell cycle analysis by FACS. Three μM H1152P but not 300 nM fully blocked proliferation and increased the number of bi-nucleated as well as of G2M-arrested cells by around 3-fold (Fig. 4E-G). This was accompanied by an increase in apoptosis (Fig. 4H), which might be due to inhibition of cytokinesis. We next

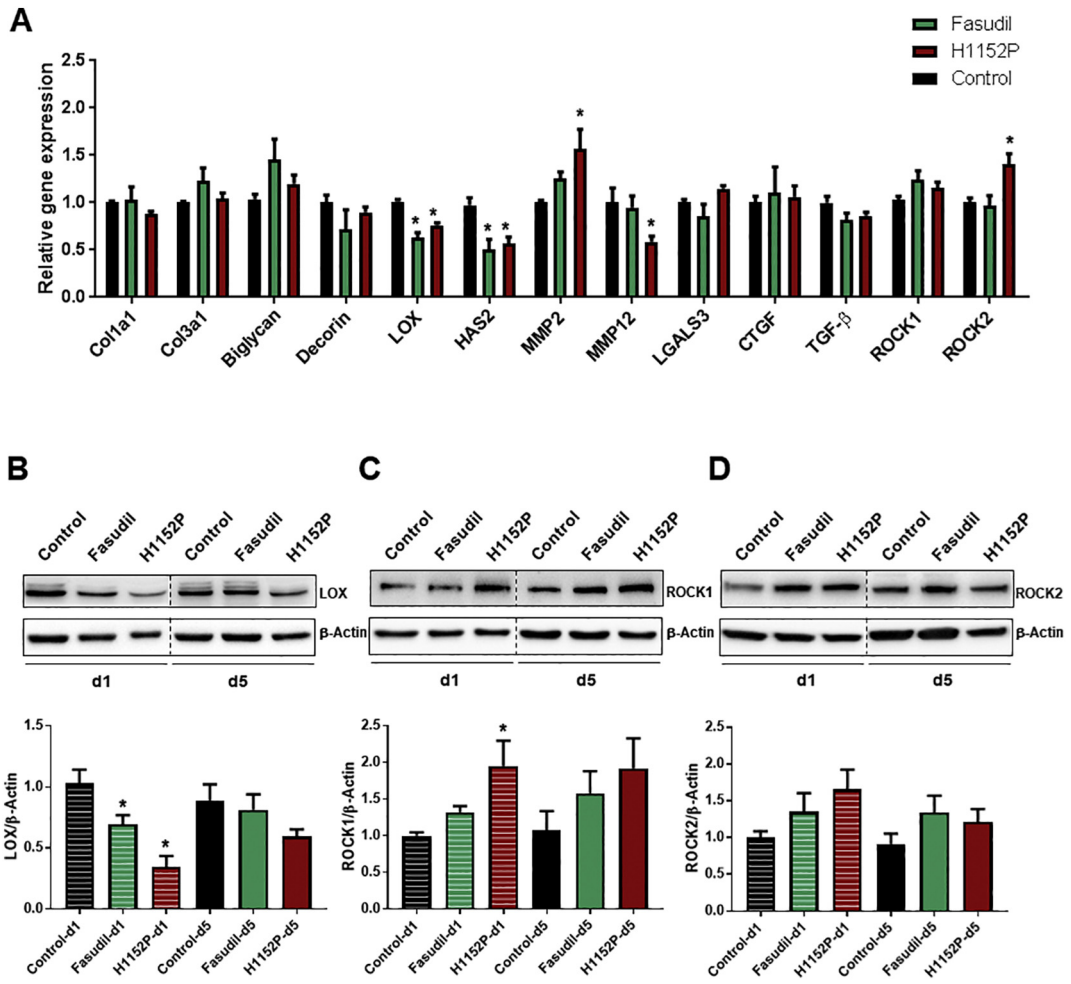

Fig. 3. ROCK inhibition regulates LOX expression in rECT. rECT were generated with NRCF and collagen I and were cultured in the absence (Control) or presence of 10 μM Fasudil or 3 μM H1152P. A) After 5 days in culture, RNA was isolated from rECT and subjected to qPCR analysis. In total RNA from 3 to 8 independent samples were analysed. All values are normalized to the mean of the housekeeping genes porphobilinogen deaminase and β-glucuronidase. Given are the means + SEM and the differences were evaluated by 2-way-ANOVA, $*p < .05$ vs. Control. B-D) After 1 day (d1) and 5 days (d5) of treatment rECT were homogenized and protein levels of LOX (B), ROCK1 (C) and ROCK2 (D) were detected by immunoblot analyses. Shown are representative immunoblots (upper panel) and the quantification of 3 independent experiments in which at least 7 rECT were investigated. The data is given normalized by β-actin and relative to control at day 1 as mean + SEM. Differences were evaluated by 1-way-ANOVA, $*p < .05$ vs. Control-d1.

determined the effect of H1152P on gene expression in 2D cultures after 48 h and 5 days of treatment (Fig. 5). LOX RNA levels were concentration-dependently decreased in H1152P-treated cells after 48 h and 5 days (Fig. 5A). The respective protein levels showed similar changes, however being only significant after 48 h. LOX expression was lower after 5 days compared to 48 h in controls and in the presence of 300 nM H1152P (Fig. 5F, G). To validate the inhibition of ROCK, we further investigated the expression of α-smooth muscle-actin (SMA), a known target of the RhoA/ROCK pathway [35]. Comparable to LOX, SMA was reduced on RNA level at both time points (Fig. 5B) as well as in rECT after 5 days (Fig. 5C). SMA protein was also significantly reduced after 48 h. In contrast to LOX, SMA expression tends to increase over the 5 days culture period (Fig. 5F, H). ROCK1 and ROCK2 RNA levels showed at 3 μM H1152P an inverse regulation at the two different time points (Fig. 5D, E). On protein level only the moderate increase after 48 h was consistent with the RNA data (Fig. 5F, I, J). We further investigated potential changes in the RNA levels of Col1a1, Col3a1, HAS2, MMP2 and MMP12 after 48 h and 5 days of treatment. (Suppl.-Fig. 2). Similar to the rECT model, both collagens were not regulated (Suppl.-Fig. 2A, 2B) and after 5 days of treatment HAS2 was decreased and MMP2 increased (Suppl.-Fig. 2C, 2D). MMP12 showed in 2D culture an opposite regulation compared to rECT (Suppl.-Fig. 2E).

3.5. Inhibition of actin polymerization and MRTF translocation reduced rECT compaction and stiffness as well as LOX expression

The expression of LOX was suggested to be regulated by the actin-dependent MRTF/SRF activation, which is a known RhoA/ROCK pathway [35,36]. We therefore tested next the impact of the actin polymerization inhibitor LatA and the MRTF translocation inhibitor CCG-203971 on rECT properties and on the expression of LOX [37]. Both treatments reduced rECT compaction (Fig. 6A, B) and stiffness (Fig. 6C, D) with LatA showing the more pronounced effect. Neither LatA nor CCG-203971 affected the rECT extensibility (Fig. 6E). Importantly, LatA and CCG-203971 reduced the expression of LOX in rECT significantly after 5 days of treatment (Fig. 6F). This data supports the hypothesis that ROCK regulates LOX expression via the actin/MRTF/SRF pathway.

3.6. LOX inhibition resembles the effect of ROCK inhibition on rECT stiffness

As described above, inhibition of ROCK, of actin polymerization, and of MRTF translocation consistently reduced LOX expression in rECT. We therefore analysed the impact of LOX inhibition by BAPN on

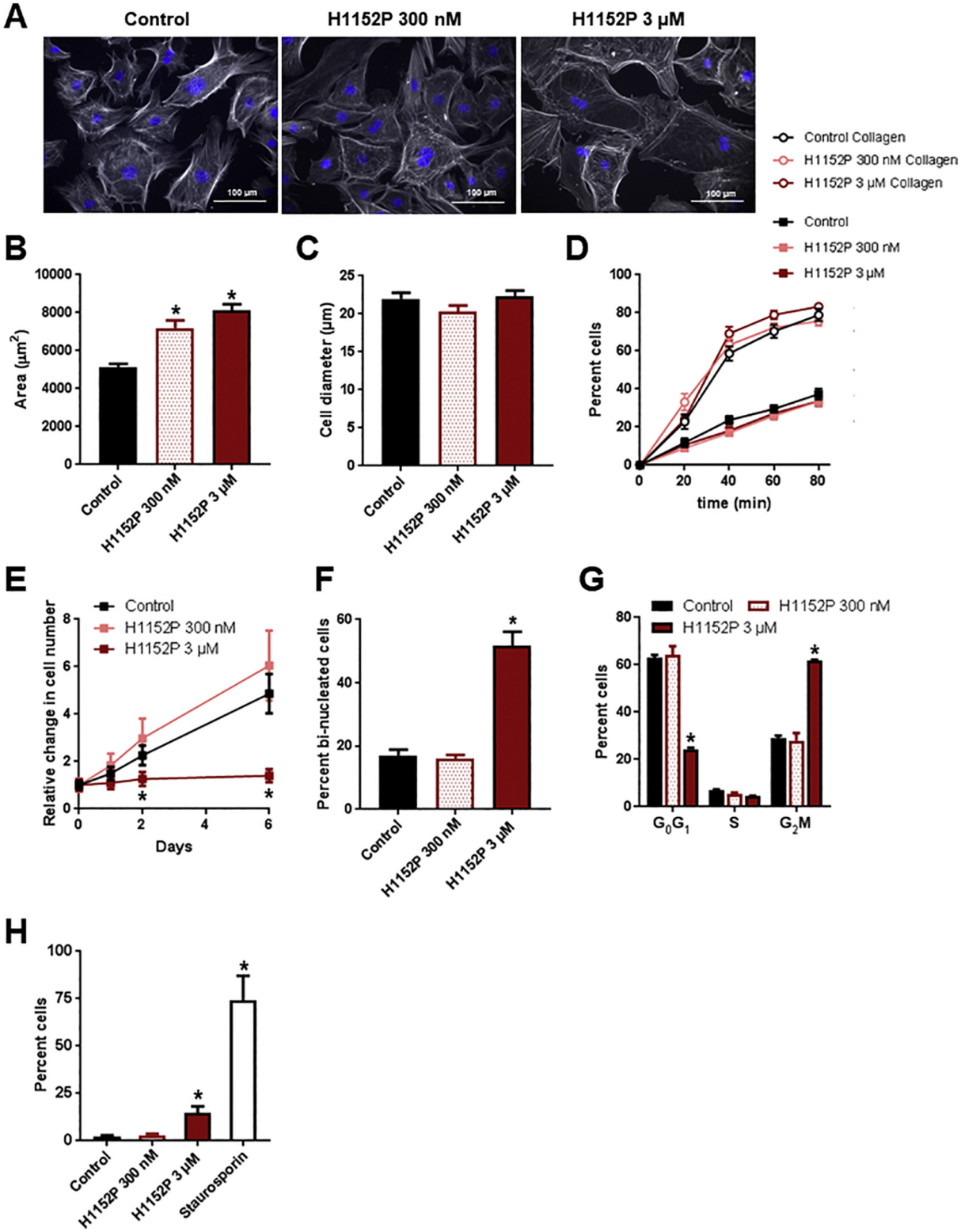

(caption on next page)

the morphology of rECT. BAPN alone had no effect on tissue compaction and did not alter the inhibitory effect of H1152P on tissue compaction (Fig. 7A, B). By contrast, BAPN reduced tissue stiffness in a similar way to H1152P. The combined application of both inhibitors showed no additive effect on tissue stiffness (Fig. 7C, D). Similar to H1152P, BAPN did not impair cell viability, as determined from cells isolated from rECT (Fig. 7E, F). Cell cycle analysis of the re-isolated cells verified the increase in the percentage of G2M phase cells after H1152P treatment (see Fig. 1J). This was not an indirect consequence of the decrease in tissue stiffness, as BAPN treatment did not alter cell cycle distribution (Fig. 7G). Moreover, BAPN alone did not alter the transcription of SMA and LOX (Fig. 7H) supporting the role of ROCK in their regulation. These findings indicate that the ROCK-dependent regulation of LOX result in changes in tissue stiffness, but not in tissue

Fig. 4. ROCK inhibition alters NRCF cell shape, cell cycle progression and LOX expression in 2D cultures. NRCF were treated with the indicated concentration of H1152P and subjected to the respective analyses. A) The treated NRCF were fixed after 48 h and stained with FITC-phalloidin (gray) and DAPI (blue). Images were taken with a 20× objective and a fluorescence microscope. Shown are representative merges of both channels. B) Based on the FITC-phalloidin images the areas of attached cells were determined. Given are the means + SEM of 3 independent experiments. The differences were evaluated by 1way-ANOVA, *p < .05 vs. Control. C) The treated NRCF were detached and the cell diameters were determined with the help of the Casy TT system. Given are the means + SEM of 3 independent experiments. D) The pre-treated, detached NRCF were seeded in 12-well plates in the absence or presence of a collagen I coat. Images were taken every 20 min and the percentage of attached cells was determined. Given are the means ± SEM of 3 independent experiments. E) The NRCF were seeded in cell culture plates, treated with the indicated concentrations of H1152P and fixed 24 h after seeding (Day 0) as well as 1, 2 and 6 days later. The nuclei were stained with DAPI and counted automatically. Given are the means ± SEM of 5–6 independent experiments. The differences were evaluated by 2way-ANOVA, *p < .05 vs. Control. F-G) The NRCF were treated for 48 h, detached, fixed, stained and subjected to FACS analysis. The numbers of bi-nucleated cells (F) and of cells in different cell cycle phases (G) were analysed. Given are the means + SEM of 4–6 independent experiments. The differences were evaluated by 1way- (F) or 2way ANOVA (G), *p < .05 vs. Control. H) The NRCF were treated for 48 h as indicated and apoptotic cells were identified by a life cell annexin V/propidium iodide stain. The percentages of apoptotic cells are given as means + SEM of 3 independent experiments. The differences were evaluated by 1way-ANOVA, *p < .05 vs. Control. (For interpretation of the references to colour in this figure legend, the reader is referred to the web version of this article.)

compaction.

3.7. ROCK inhibition reduced compaction and stiffness of hECT

To ensure that the observed ROCK inhibitor-induced decrease in rECT compaction and stiffness is not species-specific or dependent on the maturation state of the cells, we generated hECT from normal adult human ventricular cardiac fibroblasts and bovine collagen I. The tissues were treated with 10 μM Fasudil or 3 μM H1152P. Comparable to the rat tissues, the ROCK inhibitor-treated hECT showed decreased compaction (Fig. 8A, B) as well as a strong reduction in tissue stiffness represented by the significantly lower Young's moduli (Fig. 8C, D). A slight increase in the extensibility of H1152P-treated hECT was found (Fig. 8E). In line with our findings for rECT, H1152P exhibited a stronger effect than Fasudil. ROCK inhibition by Fasudil or H1152P in hECT also resulted in a reduction of LOX gene transcription and protein expression (Fig. 8F, G).

3.8. ROCK inhibition reduces stiffness of rEHM

Finally, we wanted to know if the observed differences in control and ROCK inhibitor-treated ECT translate into heterocellular rat engineered heart muscle (rEHM). We therefore generated rEHM which were cultured for the last 7 days in the presence of either 10 μM Fasudil or 3 μM H1152P. Similar to the ECT experiments, both ROCK inhibitors significantly increased the cross-sectional areas of rEHM (Fig. 9A, B). Next, we performed isometric force measurements and found that ROCK inhibition reduced the resting tension of the rEHM reflecting a decline in tissue stiffness (Fig. 9C). Interestingly, there was a trend towards an increase in twitch tension of the rEHM (Fig. 9D). As the degree of calcium sensitivity of rEHM is a measure of cardiomyocyte maturation [38], we determined the EC_{50} values of the calcium-dependent contractile response of the rEHM, but could not detect any difference between the groups (Fig. 9E). As this argued for an improvement of the contractile function due to better tissue compliance, we further subjected the rEHM to rheology. This confirmed that the stiffness of the Fasudil and H1152P-treated rEHM was reduced as shown by representative stress-strain curves (Fig. 9F) and the lower Young's moduli (Fig. 9G). Similar to rECT, no significant change in tissue extensibility was found (Fig. 9H).

4. Discussion

In diverse animal models it was demonstrated that ROCK1 or ROCK2 deletion as well as their simultaneous inhibition result in a suppression of fibrotic processes in response to heart stress [8,10,12,39–41]. The extensive intercellular communication in these models makes it however impossible to discriminate between auto-, para- and endocrine effects, and thus to delineate the role of ROCKs in different cardiac cell types. Moreover, animal models are not suitable to study the effect of a certain protein on distinct cellular processes taking place in cardiac fibrosis including fibroblast proliferation and contraction as well as ECM production, compression and remodelling. Mammalian models are also too elaborate to compare many different conditions or to perform extensive drug screening. These hurdles prompt many researchers to study, solely or additionally, cardiac fibroblast behaviour in homogenous 2D cultures, which bear the disadvantage of an unnatural stiff substrate and the lack of an embedding matrix. The consequence in 2D is a fast transition of isolated cardiac fibroblasts into myofibroblasts, which are likely different from their matrix-embedded counterparts. We found in our study substantial differences between cells in 2D culture and the embedded cells, which still represent myofibroblasts based on their expression of SMA. One intriguing example is given by the cell cycle experiments. In 2D cultures around 60% of the cells were found to be in G0G1 phase, in ECT around 90% of the cells were in this phase indicating that the 3D environment reduces the proliferation capacity of myofibroblasts.

Taking these problems into consideration, we believe that tissue engineering offers several advantages in the research field of cardiac fibrosis. Especially, the use of ECT is a straightforward approach. ECT can be prepared in a very short time with cells from different origins and maturation states and in different scales. Fibrotic stimuli like TGF-β as well as anti-fibrotic substances can be easily applied and investigated. The low number of necessary cells makes it possible to study different substances at the same time or in varying concentrations. This allowed us to compare the effects of Fasudil and H1152P, to demonstrate the concentration-dependent effect of SR-3677, to confirm that ROCKs play a role downstream of TGF-β in cardiac fibroblasts behaviour as suggested before [10], and to validate the importance of ROCK-dependent signalling events like the actin-MRTF-LOX regulation. In addition to the presented pharmacological study we have demonstrated in the past that ECT can be prepared from male and female cells to study sex-differences in cardiac fibrosis and from virally transduced cells allowing loss- and gain-of function studies [15,18,30,42].

The ECT model is not only flexible in its composition, but also in its functional readout possibilities. Besides the analyses of gene expression, cell viability and cell cycle, the most important readout is the determination of the biomechanical properties. We performed ultimate destructive tensile measurements in order to obtain information on the tissue stiffness (Young's modulus) and on the strain to failure point reflecting the maximal extensibility of a tissue. Both parameters are independent of each other and are likely important for the consideration whether or not a treatment or intervention is worth to follow-up in more elaborate pre-clinical studies. This raises the question of how a promising treatment should influence the biomechanics of ECT. It is important to understand that our ECT model is a disease models as the mean stiffness of the control tissues are around 10 times higher as the reported values for healthy mammalian hearts [43,44]. One basic requirement is therefore that an intervention reduces the stiffness of the engineered tissue towards normal. In contrast, this intervention should not negatively affect the extensibility of the tissues as this gives reason to suspect that it could result in the structural disintegration of the

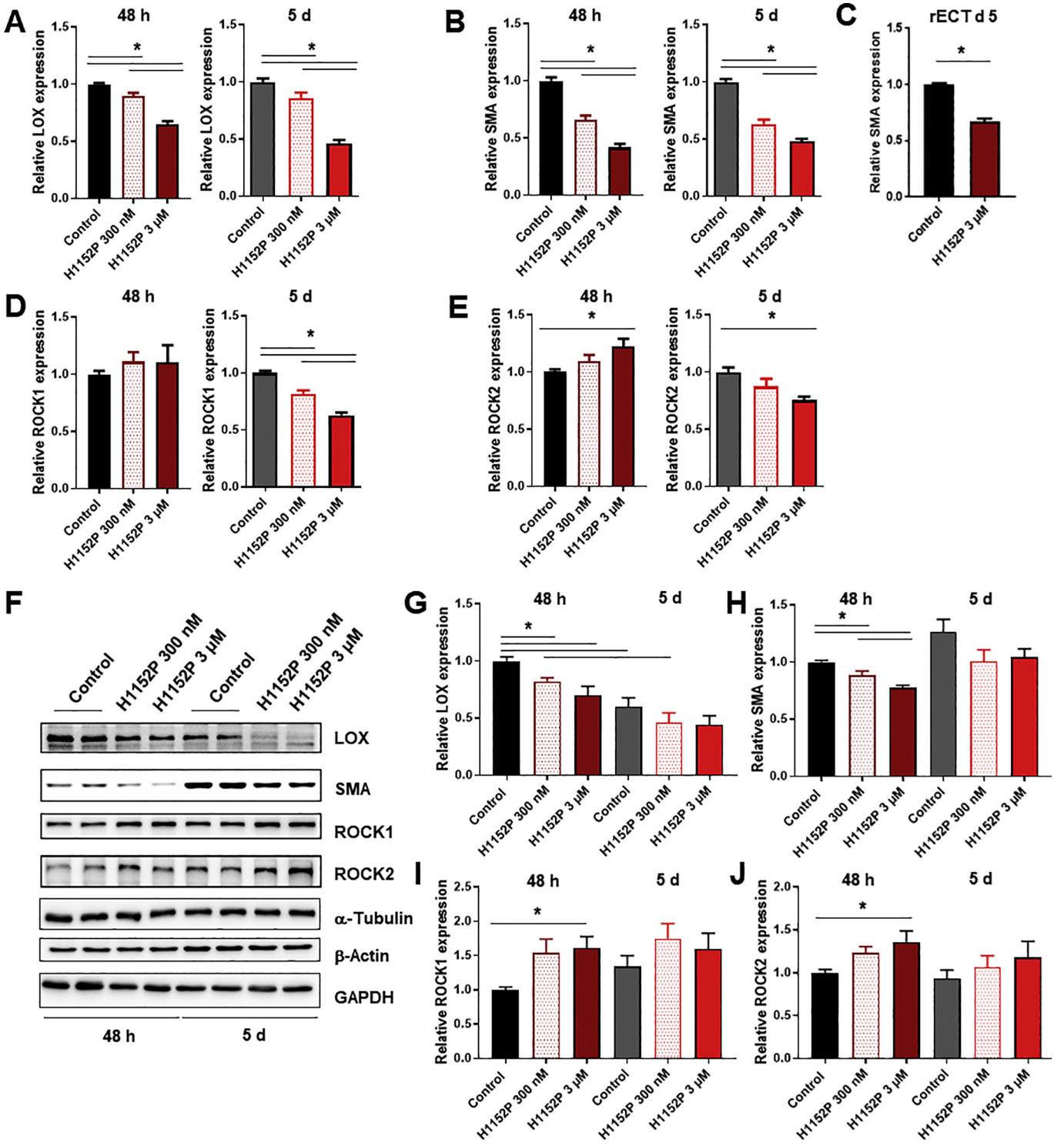

Fig. 5. ROCK inhibition regulates LOX and SMA expression in 2D NRCF cultures. RNA and protein were extracted from NRCF treated for 48 h and 5 d with 300 nM or 3 μM H1152P and subjected to qPCR and immunoblot analyses. The following transcripts and proteins were analysed: LOX (A, G), SMA (B, H), ROCK1 (C, I), ROCK2 (D, J). SMA transcription was additionally analysed in rECT (C). A-E) All qPCR values were normalized to the mean of the housekeeping genes porphobilinogen deaminase and hypoxanthine phosphoribosyltransferase 1 and are given relative to control. In total RNA from 4 independent experiments were analysed. Shown are the means + SEM. The differences were evaluated by 1-way-ANOVA or an unpaired *t*-test (ECT), $*p < .05$. F) Representative immunoblots of LOX, SMA, ROCK1, ROCK2 and of the housekeeping proteins α-tubulin, β-actin and GAPDH are shown. G-J) Protein levels were normalized by the housekeeping proteins and are given relative to control 48 h as means + SEM of 4 independent experiments. The differences were evaluated by 1-way-ANOVA, $*p < .05$.

myocardium in vivo.

We used in our study three different ROCK inhibitors, which displayed all similar effects on ECT properties, however, with different potencies. Among the isoquinoline inhibitors, H1152P reduced more potently tissue compaction and stiffness than Fasudil, which is in line with their reported K_i and IC_{50} values. In general, the published IC_{50} values of both inhibitors are substantially higher as their K_i value and seem to vary dependent on the cell type and the investigated effect.

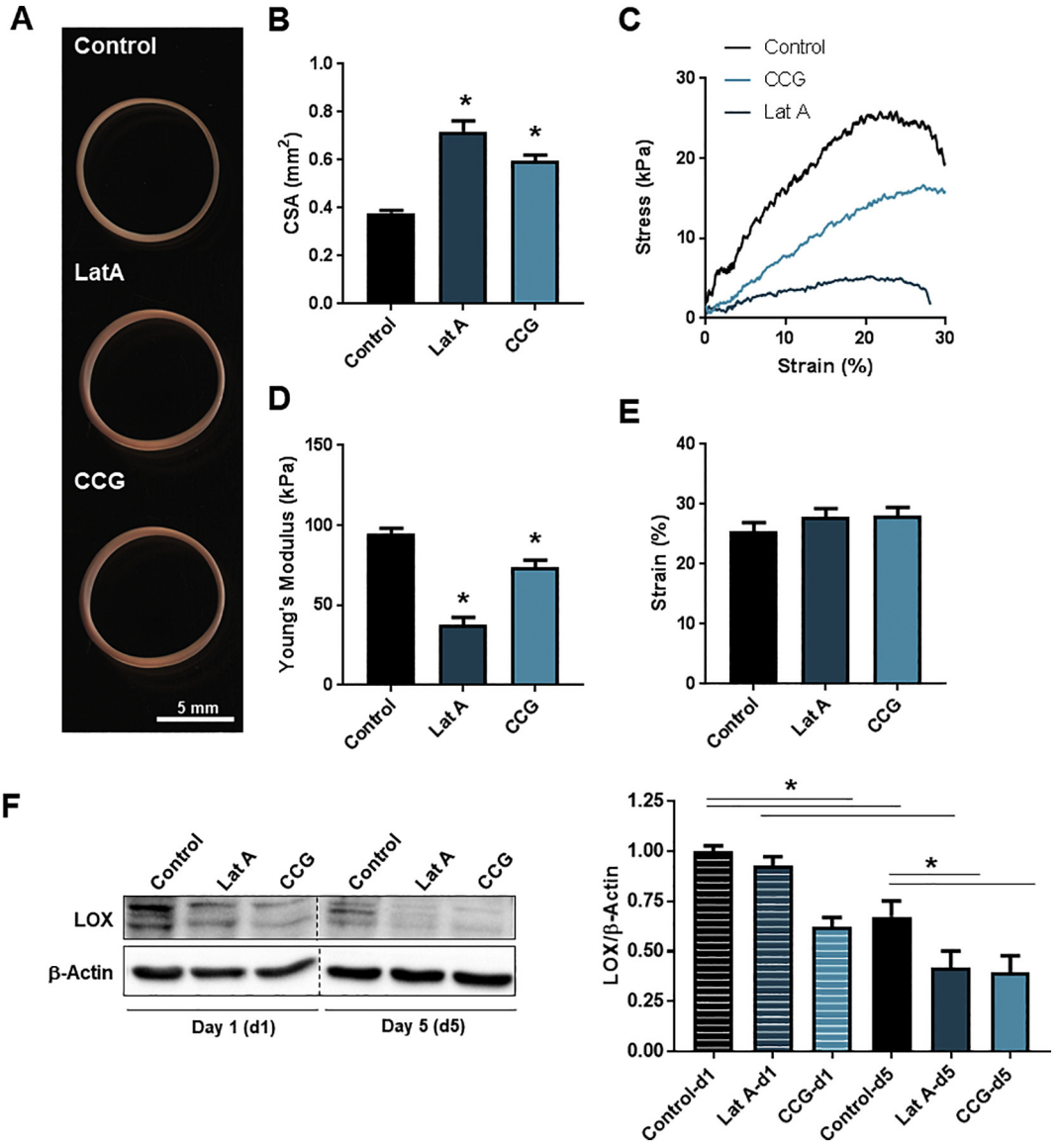

Fig. 6. Inhibition of actin polymerization and MRTF translocation reduced rECT compaction and stiffness as well as LOX expression. rECT were generated with NRCF and collagen I and were cultured for 5 days in the absence (Control) or presence of 7 ng/mL LatA or 50 μM CCG-203971. A) Representative images of rECT are shown. B) The cross sectional areas (CSA) were determined by image analysis. Given are the means ± SEM of 16 individual tissues from 3 independent experiments. Differences were analysed by 1way-ANOVA, $*p < .05$ vs. Control. C) Representative stress-strain curves from destructive tensile measurements are shown. D-E) The Young's moduli (D) and the strain to failure point (E) were extracted from the obtained stress-strain curves. Given are the means + SEM of 16 individual tissues from 3 independent experiments. Differences were analysed by 1way-ANOVA, $*p < .05$ vs. Control. F) Proteins were extracted from rECT treated for 1 or 5 days and subjected to immunoblot analysis. Shown are representative immunoblots of LOX and β-actin (left). LOX expression was normalized to β-actin expression and is given relative to Control-d1. The values are means + SEM of 4 independent experiments (right). Differences were analysed by 1way-ANOVA, $*p < .05$.

Moreover, the relative differences between K_i and IC_{50} are not identical as the K_i values differ by 200-fold (Fasudil K_i 330 nM, H1152P K_i 1.6 nM) [32] and the IC_{50} by around 2 to 20-fold in comparative studies (Fasudil IC_{50} range 2 μM–10 μM, H1152P IC_{50} range 200 nM-2 μM) [45–48]. Based on these published values, we decided to use in our study inhibitor concentrations which are close to the reported maximal IC_{50} values in order to minimize off-target effects, but which still allow sufficient inhibition. Under these conditions both inhibitors fulfilled the requirement of reducing the stiffness of rECT to values published for the normal rat heart [43] and importantly without affecting the tissue extensibility. In hECT, however, both inhibitors were not as effective in stiffness reduction and thus didn't meet the criteria. In comparison to Fasudil and H1152P, the pyrazol-phenyl inhibitor SR-3677 was most potent in reducing rECT compaction and stiffness. The IC_{50} for the decline in the Young's modulus was around 10 nM, which is 3 times above the reported IC_{50} for ROCK2 and 5 times below the IC_{50} of ROCK1 [34], which might indicate that ROCK2 is more important for tissue stiffening that ROCK1. Future studies are needed to validate the isoform-specificity, the potential therapeutic value and the off-target effects of SR-3677. This is also true for the many new ROCK inhibitors, which have been developed in the last few years, mainly driven by their promising therapeutic effect in the treatment of glaucoma [49]. Independent of their chemistries, they all act as ATP competitors, and thus off-target effects are almost inevitable. In general, off-target effects are often responsible for adverse actions of a drug, but they can also directly hamper the desired effect. For example, Fasudil displays a difference in its inhibitory potency between ROCK and PKA of only 10- to 20-fold and thus partial PKA inhibition is likely when Fasudil is used [50,51]. Combined inhibition of ROCK and PKA might be, however, counter-productive in the context of cardiac fibrosis. In line with this

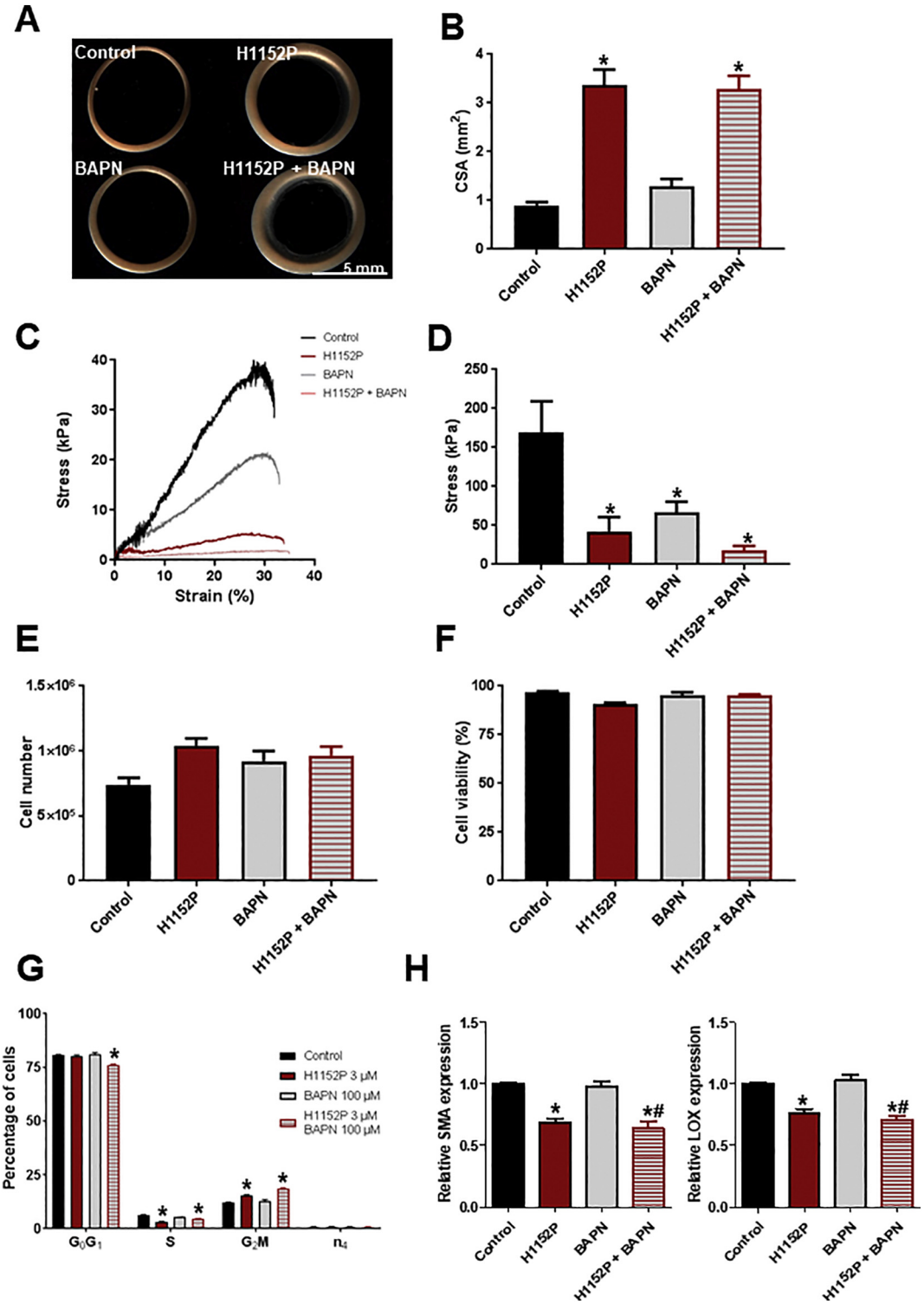

Fig. 7. LOX inhibition resembles the effect of ROCK inhibition on rECT. rECT were generated with NRCF and collagen I and were cultured for 5 days in the absence (Control) or presence of 3 µM H1152P and/or 100 µM BAPN. A) Representative images of rECT are shown. B) The cross sectional areas (CSA) were determined by image analysis. Given are the means + SEM of 12 individual tissues from 4 independent experiments. Differences were analysed by 1way-ANOVA, *$p < .05$ vs. Control. C) Representative stress-strain curves from destructive tensile measurements are shown. D) The Young's moduli were calculated based on the obtained stress-strain curves. Given are the means + SEM of 12 individual tissues from 4 independent experiments. Differences were analysed by 1way-ANOVA, *$p < .05$ vs. Control. *E*-F) The NRCF were re-isolated from rECT and the cell number (E) and viability were measured with the Casy TT system. Given are the means + SEM of 3 independent experiments. G) Cell cycle distribution was analysed by FACS in re-isolated, fixed and stained cells. Given are the percentages of cells at G0/G1, S and G2/M stages as means + SEMs of 4 independent experiments measured each in 3 technical replicates, *$p < .05$ vs. Control as assessed by 2way ANOVA. H) RNA was isolated from rECT and subjected to qPCR analysis. In total RNA from 12 rECT was analysed. All values are normalized to the mean of the housekeeping genes porphobilinogen deaminase and hypoxanthine phosphoribosyltransferase 1. Shown are the means + SEM and the differences were evaluated by 1-way-ANOVA, *$p < .05$ vs. Control, $^{\#}p < .05$ vs. BAPN.

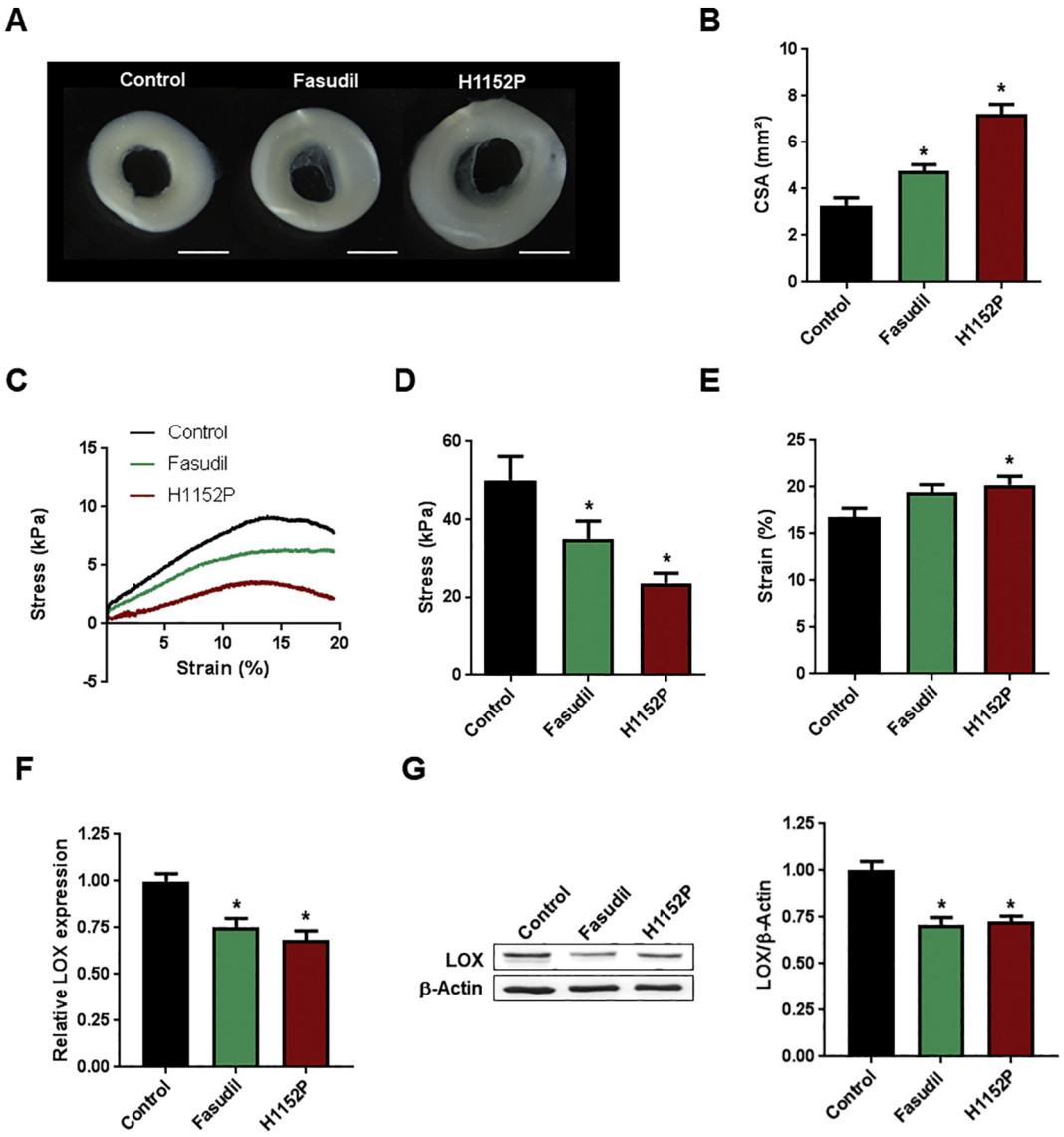

Fig. 8. ROCK inhibition reduced compaction and stiffness of hECT. hECT were prepared from normal adult human ventricular cardiac fibroblasts and collagen I. The hECT were cultured for 5 days in the absence (Control) or presence of 10 μM Fasudil or 3 μM H1152P. A) Representative images of hECT are given. B) The cross sectional areas (CSA) were determined by image analysis. Given are the means + SEM of 18 to 20 individual tissues from at least 3 independent experiments. Differences were analysed by 1way-ANOVA, $*p < .05$ vs. Control. C) Representative stress-strain curves from destructive tensile measurements are shown. D) The Young's moduli were calculated based on the obtained stress-strain curves. Given are the means + SEM of 16–20 hECT from 5 independent experiments. Differences were evaluated by 1way-ANOVA, $*p < .05$ vs. Control. E) The strain to failure point was extracted from the obtained rheology data. Given are the means ± SEM of 16–20 hECT from 5 independent experiments. F) RNA from 3 independent experiments was analysed. All values are normalized to the mean of the housekeeping genes porphobilinogen deaminase and hypoxanthine phosphoribosyltransferase 1. Shown are the means + SEM and the differences were evaluated by 1way-ANOVA, $*p < .05$ vs. Control.

hypothesis it was shown by up-stream activation of PKA and its direct inhibition, that PKA possesses certain anti-fibrotic properties in rat cardiac fibroblasts [52]. Moreover, we demonstrated earlier that the augmented degradation of cAMP by overexpression of phosphodiesterase 2 (PDE2) resulted in an enhanced cardiac fibroblast to myofibroblast conversion and an increased stiffness of rECT [42]. We therefore believe that identifying a highly specific ROCK inhibitor is crucial for taking ROCK inhibition forward into clinical studies on fibrosis in the future.

It is, however, clear that drug testing in a homogeneous cardiac fibroblast models is not sufficient to estimate its therapeutic potential. Besides the above mentioned criteria on tissue stiffness and extensibility, a further requirement is that a drug does not interfere with the contractile behaviour of cardiomyocytes. The EHM model offers here a similar fast and simple approach to test for this requirement. By using this model, we could show that ROCK inhibition induced similar effects on rEHM stiffness and compaction as found for rECT, implying that cardiac fibroblasts are the main target affecting both processes. Importantly, ROCK inhibition did not negatively interfere with the contractile function of the EHM, but showed by trend a slight improvement. Due to the unchanged calcium sensitivity, we believe that this improvement is more likely based on a better diastolic compliance of the tissues than on molecular changes in the excitation-contraction coupling in cardiomyocytes, which was described to be a potential consequence of ROCK inhibition [53,54]. Similar as found in ECT, ROCK inhibition did not affect tissue extensibility. This could explain why despite its anti-fibrotic effect ROCK inhibition was not associated with an increase in ventricular rupture after myocardial infarction in animals [55–57]. Taken together our data fuel the idea that the inhibition of ROCK could be an effective therapeutic option for diastolic

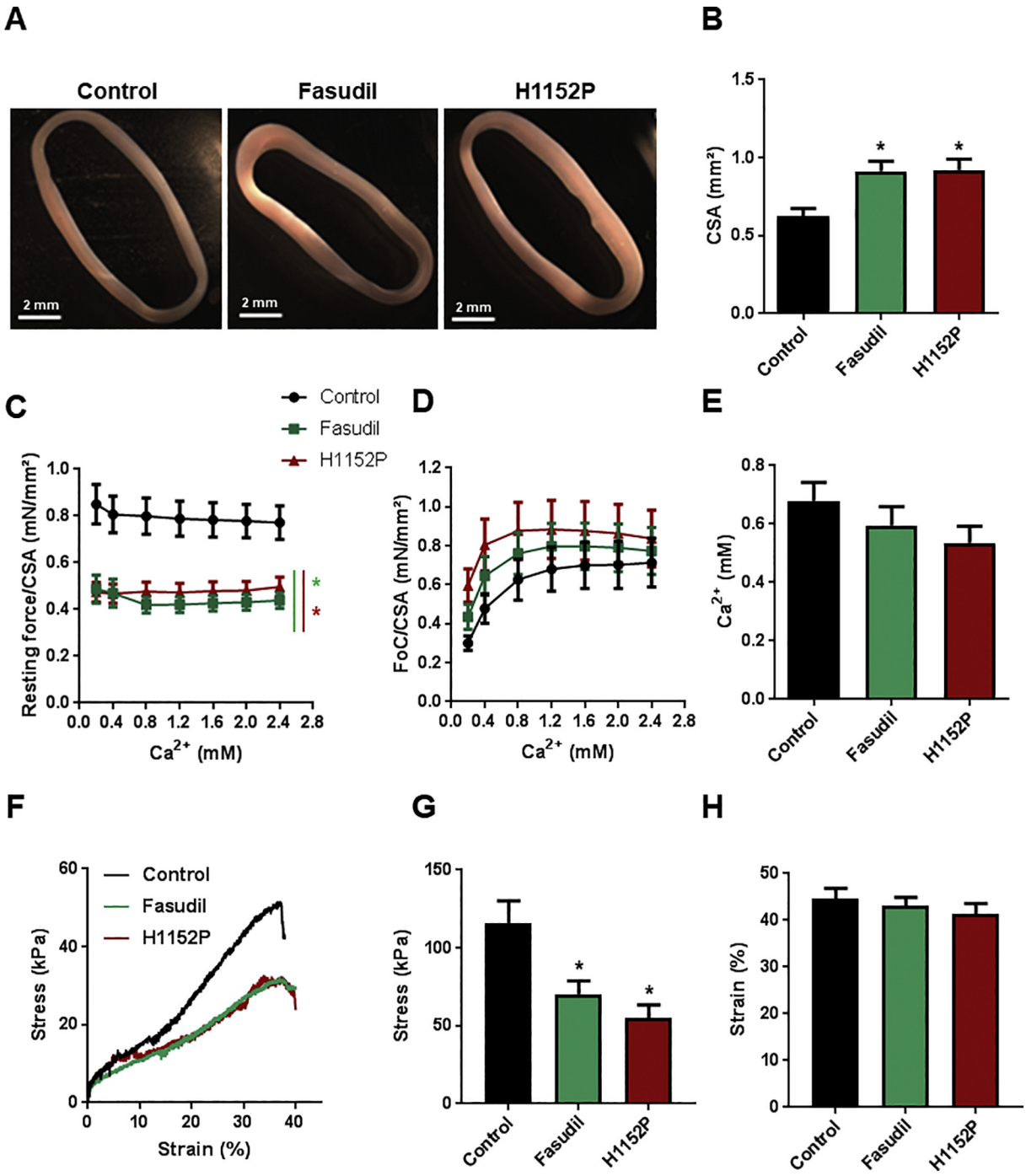

Fig. 9. ROCK inhibition reduced tissue stiffness of rEHM. rEHM were prepared from total neonatal cardiac cells and cultured for 7 days until they were fully consolidated and then transferred onto phasic stretchers for mechanical load for further 7 days. During this phase, the rEHM were treated with 10 μM Fasudil or 3 μM H1152P. A) Shown are representative images of control-, Fasudil-, and H1152P-treated rEHM. B) Differences in calculated cross sectional areas (CSA) of the rEHM are shown as means + SEM of 23 to 28 rEHM resulting from 5 independent cell isolations. C-D) Isometric force measurements were performed in an organ bath in the presence of increasing concentrations of calcium. C) The resting forces and D) contraction forces normalized by the CSA are given as means ± SEM of 29–31 rEHM from 5 independent experiments. Differences were evaluated by 2way-ANOVA, *$p < .05$ vs. Control. E) The EC_{50} values for the calcium sensitivity of the contractile function were calculated based on the measured contraction forces/CSA. F) The rEHM were further subjected to destructive tensile measurements. Representative stress-strain curves are depicted. G) The Young's moduli were calculated based on the obtained stress-strain curves. Given are the means + SEM of 13–20 rEHM from at least 3 independent experiments. The differences were evaluated by 1-way-ANOVA, *$p < .05$ vs. Control. H) The strain to failure point was calculated based on the obtained rheology data. Given are the means + SEM of 13–20 rEHM from 3 independent experiments.

dysfunction of the heart. This is supported by animal studies and preliminary clinical trials. For example, in a pressure overload rat model the ROCK inhibitor GSK-57637 significantly attenuated diastolic dysfunction. Interestingly, the ACE inhibitor Ramipril was not as effective as GSK-57637 [58]. Moreover, deletion of ROCK2 from cardiac myofibroblasts in mice reduced the diastolic dysfunction after chronic Ang II treatment [10]. Finally, in two clinical studies Fasudil was shown to improve diastolic dysfunction in patients with Diabetes type 2 and in patients with reactive pulmonary hypertension both associated with left ventricular impairment, but with preserved ejection fraction [59,60].

Our work highlights not only ROCK inhibition as an interesting therapeutic option but also contributes to the understanding of the underlying mechanisms. In former studies the anti-fibrotic effect of ROCK inhibitors or ROCK deletion has been attributed to their ability to reduce the expression of fibrosis-associated genes [61]. Our results show that ROCK inhibition has little effect on the transcription of pro-fibrotic genes and regulators of the cardiac fibroblast ECM when embedded in a 3D matrix. We found no change in Col1a1, Col3a1, Biglycan, Decorin, LGALS3, CTGF, and TGF-β transcription, an up- and down-regulation regulation of MMP2 and MMP12 by H1152P only, and a down-regulation of HAS2 and LOX by both inhibitors. We could confirm by 2D cultures that LOX expression is reduced after 48 h on RNA and protein level as well as on protein level in the ECT after 1 day treatment. The changes in LOX protein levels after 5 days were not as pronounced as after shorter incubation periods. Similar reductions in LOX gene transcription as a consequence of ROCK inhibition has been reported before. It was shown that Y27632 reduced LOX RNA in NIH3T3 fibroblasts [62], Fasudil in astrocytes [63], and SLx-2119 in human pulmonary artery smooth muscle cells as well as human dermal fibroblasts [64]. This led us to the hypothesis that LOX is not only regulated by Hif1α [65,66], peroxisome proliferator-activated receptor γ [67], SMAD 2/3 and AP1 [68], as well as by the nuclear factor I [69], but also by the RhoA/ROCK-regulated, actin-dependent MRTF/SRF transcriptional complex [70,71]. In line with this hypothesis, it has been demonstrated by ChIP- and RNA-sequencing that the MRTF/SRF transcriptional complex binds in a serum-dependent manner in proximity to the LOX gene and that serum induces LOX transcription dependent on actin [36]. As the functionality of this pathway has never been tested before, we treated our rECT with the actin polymerization inhibitor LatA or the MRTF translocation inhibitor CCG-20397. Both substances interfered with tissue compaction and stiffness and most importantly they reduced the expression of LOX. We therefore tested next the effect of the inhibition of LOX and likely of LOX homologs (LOX-like 1-4) by the pan-inhibitor BAPN [72,73] and found that it mimicked the phenotype of ROCK inhibition with respect to ECT stiffness. This anti-fibrotic effect of BAPN is in line with data from several in vivo studies. For example, BAPN treatment was found to reduce left ventricular stiffness and collagen content in a volume overload rat model [74,75], to diminish the extent of cardiac fibrosis in rats subjected to a high fat diet [76], and to attenuated cardiac fibrosis and ventricular dilatation in a murine myocardial infarction model [77].

In summary, we have shown that our two-tiered engineered tissue approach offers several advantages in drug testing and signal pathway delineation in the setting of cardiac fibrosis. We found that ROCK inhibition, partly via reducing LOX expression, offers an interesting therapeutic approach for cardiac fibrosis.

Acknowledgements

This work was funded by the German Research Foundation by projects IRTG 1816 RP8 to SH and GS, DZHK (German Center for Cardiovascular Research) to SL (81X2300161), and Cancer Research UK C6620/A15961 to AJR. WHZ is supported by the DZHK and the German Research Foundation (DFG ZI 708/10-1, SFB 1002 TP C04, S01, SFB 937 TP A18, IRTG 1816 RP12). This study reports the results of the doctoral theses of SH and GS, both members of the IRTG 1816.

References

[1] T.M. Hale, Persistent phenotypic shift in cardiac fibroblasts: impact of transient renin angiotensin system inhibition, J. Mol. Cell. Cardiol. 93 (2016) 125–132.
[2] O. Kanisicak, H. Khalil, M.J. Ivey, J. Karch, B.D. Maliken, R.N. Correll, M.J. Brody, J.L. SC, B.J. Aronow, M.D. Tallquist, J.D. Molkentin, Genetic lineage tracing defines myofibroblast origin and function in the injured heart, Nat. Commun. 7 (2016) 12260.
[3] X. Fu, H. Khalil, O. Kanisicak, J.G. Boyer, R.J. Vagnozzi, B.D. Maliken, M.A. Sargent, V. Prasad, I. Valiente-Alandi, B.C. Blaxall, J.D. Molkentin, Specialized fibroblast differentiated states underlie scar formation in the infarcted mouse heart, J. Clin. Invest. 128 (5) (2018) 2127–2143.
[4] J. Zent, L.W. Guo, Signaling mechanisms of myofibroblastic activation: outside-in and inside-out, Cell. Physiol. Biochem. 49 (3) (2018) 848–868.
[5] S.E. Campbell, J.S. Janicki, K.T. Weber, Temporal differences in fibroblast proliferation and phenotype expression in response to chronic administration of angiotensin II or aldosterone, J. Mol. Cell. Cardiol. 27 (8) (1995) 1545–1560.
[6] S. Hartmann, A.J. Ridley, S. Lutz, The function of rho-associated kinases ROCK1 and ROCK2 in the pathogenesis of cardiovascular disease, Front. Pharmacol. 6 (2015) 276.
[7] J. Chang, M. Xie, V.R. Shah, M.D. Schneider, M.L. Entman, L. Wei, R.J. Schwartz, Activation of Rho-associated coiled-coil protein kinase 1 (ROCK-1) by caspase-3 cleavage plays an essential role in cardiac myocyte apoptosis, Proc. Natl. Acad. Sci. U. S. A. 103 (39) (2006) 14495–14500.
[8] R. Okamoto, Y. Li, K. Noma, Y. Hiroi, P.Y. Liu, M. Taniguchi, M. Ito, J.K. Liao, FHL2 prevents cardiac hypertrophy in mice with cardiac-specific deletion of ROCK2, FASEB J. 27 (4) (2013) 1439–1449.
[9] J. Shi, Y.W. Zhang, Y. Yang, L. Zhang, L. Wei, ROCK1 plays an essential role in the transition from cardiac hypertrophy to failure in mice, J. Mol. Cell. Cardiol. 49 (5) (2010) 819–828.
[10] T. Shimizu, N. Narang, P. Chen, B. Yu, M. Knapp, J. Janardanan, J. Blair, J.K. Liao, Fibroblast deletion of ROCK2 attenuates cardiac hypertrophy, fibrosis, and diastolic dysfunction, JCI Insight 2 (13) (2017).
[11] S. Sunamura, K. Satoh, R. Kurosawa, T. Ohtsuki, N. Kikuchi, M. Elias-Al-Mamun, T. Shimizu, S. Ikeda, K. Suzuki, T. Satoh, J. Omura, M. Nogi, K. Numano, M.A.H. Siddique, S. Miyata, M. Miura, H. Shimokawa, Different roles of myocardial ROCK1 and ROCK2 in cardiac dysfunction and postcapillary pulmonary hypertension in mice, Proc. Natl. Acad. Sci. U. S. A. 115 (30) (2018) E7129–E7138.
[12] Y. Rikitake, N. Oyama, C.Y. Wang, K. Noma, M. Satoh, H.H. Kim, J.K. Liao, Decreased perivascular fibrosis but not cardiac hypertrophy in ROCK1 +/− haploinsufficient mice, Circulation 112 (19) (2005) 2959–2965.
[13] R. Yang, L. Chang, S. Liu, X. Jin, Y. Li, High glucose induces Rho/ROCK-dependent visfatin and type I procollagen expression in rat primary cardiac fibroblasts, Mol. Med. Rep. 10 (4) (2014) 1992–1998.
[14] S. Luo, T.B. Hieu, F. Ma, Y. Yu, Z. Cao, M. Wang, W. Wu, Y. Mao, P. Rose, B.Y. Law, Y.Z. Zhu, ZYZ-168 alleviates cardiac fibrosis after myocardial infarction through inhibition of ERK1/2-dependent ROCK1 activation, Sci. Rep. 7 (2017) 43242.
[15] A. Ongherth, S. Pasch, C.M. Wuertz, K. Nowak, N. Kittana, C.A. Weis, A. Jatho, C. Vettel, M. Tiburcy, K. Toischer, G. Hasenfuss, W.H. Zimmermann, T. Wieland, S. Lutz, p63RhoGEF regulates auto- and paracrine signaling in cardiac fibroblasts, J. Mol. Cell. Cardiol. 88 (2015) 39–54.
[16] K. Schram, R. Ganguly, E.K. No, X. Fang, F.S. Thong, G. Sweeney, Regulation of MT1-MMP and MMP-2 by leptin in cardiac fibroblasts involves Rho/ROCK-dependent actin cytoskeletal reorganization and leads to enhanced cell migration, Endocrinology 152 (5) (2011) 2037–2047.
[17] H. Zhou, K.X. Zhang, Y.J. Li, B.Y. Guo, M. Wang, M. Wang, Fasudil hydrochloride hydrate, a rho-kinase inhibitor, suppresses high glucose-induced proliferation and collagen synthesis in rat cardiac fibroblasts, Clin. Exp. Pharmacol. Physiol. 38 (6) (2011) 387–394.
[18] A. Jatho, S. Hartmann, N. Kittana, F. Mugge, C.M. Wuertz, M. Tiburcy, W.H. Zimmermann, D.M. Katschinski, S. Lutz, RhoA ambivalently controls prominent myofibroblast characteritics by involving distinct signaling routes, PLoS One 10 (10) (2015) e0137519.
[19] C. Mauch, A. Hatamochi, K. Scharffetter, T. Krieg, Regulation of collagen synthesis in fibroblasts within a three-dimensional collagen gel, Exp. Cell Res. 178 (2) (1988) 493–503.
[20] E.L. Elson, G.M. Genin, Tissue constructs: platforms for basic research and drug discovery, Interf. Focus 6 (1) (2016) 20150095.
[21] F. Weinberger, I. Mannhardt, T. Eschenhagen, Engineering cardiac muscle tissue: a maturating field of research, Circ. Res. 120 (9) (2017) 1487–1500.
[22] M. Tiburcy, W.H. Zimmermann, Modeling myocardial growth and hypertrophy in engineered heart muscle, Trends Cardiovasc. Med. 24 (1) (2014) 7–13.
[23] T. Eschenhagen, C. Fink, U. Remmers, H. Scholz, J. Wattchow, J. Weil, W. Zimmermann, H.H. Dohmen, H. Schafer, N. Bishopric, T. Wakatsuki, E.L. Elson, Three-dimensional reconstitution of embryonic cardiomyocytes in a collagen matrix: a new heart muscle model system, FASEB J. 11 (8) (1997) 683–694.
[24] V.H. Barocas, A.G. Moon, R.T. Tranquillo, The fibroblast-populated collagen microsphere assay of cell traction force—part 2: measurement of the cell traction parameter, J. Biomech. Eng. 117 (2) (1995) 161–170.
[25] J. Yu, M.M. Seldin, K. Fu, S. Li, L. Lam, P. Wang, Y. Wang, D. Huang, T.L. Nguyen, B. Wei, R.P. Kulkarni, D. Di Carlo, M. Teitell, M. Pellegrini, A.J. Lusis, A. Deb, Topological arrangement of cardiac fibroblasts regulates cellular plasticity, Circ. Res. 123 (1) (2018) 73–85.
[26] P. Lijnen, V. Petrov, R. Fagard, In vitro assay of collagen gel contraction by cardiac fibroblasts in serum-free conditions, Methods Find. Exp. Clin. Pharmacol. 23 (7) (2001) 377–382.
[27] P. Lijnen, V. Petrov, K. Rumilla, R. Fagard, Stimulation of collagen gel contraction by angiotensin II and III in cardiac fibroblasts, J. Renin Angioten. Aldoster. Syst. 3 (3) (2002) 160–166.
[28] M.L. Burgess, W.E. Carver, L. Terracio, S.P. Wilson, M.A. Wilson, T.K. Borg, Integrin-mediated collagen gel contraction by cardiac fibroblasts. Effects of angiotensin II, Circ. Res. 74 (2) (1994) 291–298.
[29] G.I. Zahalak, J.E. Wagenseil, T. Wakatsuki, E.L. Elson, A cell-based constitutive relation for bio-artificial tissues, Biophys. J. 79 (5) (2000) 2369–2381.
[30] E. Dworatzek, S. Mahmoodzadeh, C. Schriever, K. Kusumoto, L. Kramer, G. Santos, D. Fliegner, Y.K. Leung, S.M. Ho, W.H. Zimmermann, S. Lutz, V. Regitz-Zagrosek,

Sex-specific regulation of collagen I and III expression by 17beta-estradiol in cardiac fibroblasts: role of estrogen receptors, Cardiovasc. Res. 115 (2) (2018) 315–327.
[31] W.H. Zimmermann, K. Schneiderbanger, P. Schubert, M. Didie, F. Munzel, J.F. Heubach, S. Kostin, W.L. Neuhuber, T. Eschenhagen, Tissue engineering of a differentiated cardiac muscle construct, Circ. Res. 90 (2) (2002) 223–230.
[32] M. Ikenoya, H. Hidaka, T. Hosoya, M. Suzuki, N. Yamamoto, Y. Sasaki, Inhibition of rho-kinase-induced myristoylated alanine-rich C kinase substrate (MARCKS) phosphorylation in human neuronal cells by H-1152, a novel and specific Rho-kinase inhibitor, J. Neurochem. 81 (1) (2002) 9–16.
[33] Y. Sasaki, M. Suzuki, H. Hidaka, The novel and specific rho-kinase inhibitor (S)-(+)-2-methyl-1-[(4-methyl-5-isoquinoline)sulfonyl]-homopiperazine as a probing molecule for rho-kinase-involved pathway, Pharmacol. Ther. 93 (2–3) (2002) 225–232.
[34] Y. Feng, Y. Yin, A. Weiser, E. Griffin, M.D. Cameron, L. Lin, C. Ruiz, S.C. Schurer, T. Inoue, P.V. Rao, T. Schroter, P. Lograsso, Discovery of substituted 4-(pyrazol-4-yl)-phenylbenzodioxane-2-carboxamides as potent and highly selective rho kinase (ROCK-II) inhibitors, J. Med. Chem. 51 (21) (2008) 6642–6645.
[35] L. Fan, A. Sebe, Z. Peterfi, A. Masszi, A.C. Thirone, O.D. Rotstein, H. Nakano, C.A. McCulloch, K. Szaszi, I. Mucsi, A. Kapus, Cell contact-dependent regulation of epithelial-myofibroblast transition via the rho-rho kinase-phospho-myosin pathway, Mol. Biol. Cell 18 (3) (2007) 1083–1097.
[36] C. Esnault, A. Stewart, F. Gualdrini, P. East, S. Horswell, N. Matthews, R. Treisman, Rho-actin signaling to the MRTF coactivators dominates the immediate transcriptional response to serum in fibroblasts, Genes Dev. 28 (9) (2014) 943–958.
[37] L.A. Johnson, E.S. Rodansky, A.J. Haak, S.D. Larsen, R.R. Neubig, P.D. Higgins, Novel Rho/MRTF/SRF inhibitors block matrix-stiffness and TGF-beta-induced fibrogenesis in human colonic myofibroblasts, Inflamm. Bowel Dis. 20 (1) (2014) 154–165.
[38] A.F. Godier-Furnemont, M. Tiburcy, E. Wagner, M. Dewenter, S. Lammle, A. El-Armouche, S.E. Lehnart, G. Vunjak-Novakovic, W.H. Zimmermann, Physiologic force-frequency response in engineered heart muscle by electromechanical stimulation, Biomaterials 60 (2015) 82–91.
[39] Y. Rikitake, J.K. Liao, Rho-kinase mediates hyperglycemia-induced plasminogen activator inhibitor-1 expression in vascular endothelial cells, Circulation 111 (24) (2005) 3261–3268.
[40] S.B. Haudek, D. Gupta, O. Dewald, R.J. Schwartz, L. Wei, J. Trial, M.L. Entman, Rho kinase-1 mediates cardiac fibrosis by regulating fibroblast precursor cell differentiation, Cardiovasc. Res. 83 (3) (2009) 511–518.
[41] X. Yang, Q. Li, X. Lin, Y. Ma, X. Yue, Z. Tao, F. Wang, W.L. McKeehan, L. Wei, R.J. Schwartz, J. Chang, Mechanism of fibrotic cardiomyopathy in mice expressing truncated Rho-associated coiled-coil protein kinase 1, FASEB J. 26 (5) (2012) 2105–2116.
[42] C. Vettel, S. Lammle, S. Ewens, C. Cervirgen, J. Emons, A. Ongherth, M. Dewenter, D. Lindner, D. Westermann, V.O. Nikolaev, S. Lutz, W.H. Zimmermann, A. El-Armouche, PDE2-mediated cAMP hydrolysis accelerates cardiac fibroblast to myofibroblast conversion and is antagonized by exogenous activation of cGMP signaling pathways, Am. J. Physiol. Heart Circ. Physiol. 306 (8) (2014) H1246–H1252.
[43] E.U. Azeloglu, K.D. Costa, Cross-bridge cycling gives rise to spatiotemporal heterogeneity of dynamic subcellular mechanics in cardiac myocytes probed with atomic force microscopy, Am. J. Physiol. Heart Circ. Physiol. 298 (3) (2010) H853–H860.
[44] O. Villemain, M. Correia, E. Mousseaux, J. Baranger, S. Zarka, I. Podetti, G. Soulat, T. Damy, A. Hagege, M. Tanter, M. Pernot, E. Messas, Myocardial stiffness evaluation using noninvasive shear wave imaging in healthy and hypertrophic cardiomyopathic adults, Cardiovasc. Imag. S1936-878X (18) (2018) 30140–30142.
[45] W.W. Shum, G.Y. Le, R.L. Jones, A.M. Gurney, Y. Sasaki, Involvement of Rho-kinase in contraction of Guinea-pig aorta induced by prostanoid EP3 receptor agonists, Br. J. Pharmacol. 139 (8) (2003) 1449–1461.
[46] M. Hanazaki, M. Yokoyama, K. Morita, A. Kohjitani, H. Sakai, Y. Chiba, M. Misawa, Rho-kinase inhibitors augment the inhibitory effect of propofol on rat bronchial smooth muscle contraction, Anesth. Analg. 106 (6) (2008) 1765–1771.
[47] C.E. Teixeira, L. Jin, F.B. Priviero, Z. Ying, R.C. Webb, Comparative pharmacological analysis of Rho-kinase inhibitors and identification of molecular components of Ca2+ sensitization in the rat lower urinary tract, Biochem. Pharmacol. 74 (4) (2007) 647–658.
[48] S. Rattan, C.A. Patel, Selectivity of ROCK inhibitors in the spontaneously tonic smooth muscle, Am. J. Physiol. Gastrointest. Liver Physiol. 294 (3) (2008) G687–G693.
[49] R. Nourinia, S. Nakao, S. Zandi, S. Safi, A. Hafezi-Moghadam, H. Ahmadieh, ROCK inhibitors for the treatment of ocular diseases, Br. J. Ophthalmol. 102 (2017) 1–5.
[50] S.P. Davies, H. Reddy, M. Caivano, P. Cohen, Specificity and mechanism of action of some commonly used protein kinase inhibitors, Biochem. J. 351 (Pt 1) (2000) 95–105.
[51] C. Breitenlechner, M. Gassel, H. Hidaka, V. Kinzel, R. Huber, R.A. Engh, D. Bossemeyer, Protein kinase A in complex with Rho-kinase inhibitors Y-27632, Fasudil, and H-1152P: structural basis of selectivity, Structure 11 (12) (2003) 1595–1607.
[52] Q. Wang, T. Oka, K. Yamagami, J.K. Lee, H. Akazawa, A.T. Naito, T. Yasui, T. Ishizu, Y. Nakaoka, Y. Sakata, I. Komuro, An EP4 receptor agonist inhibits cardiac fibrosis through activation of PKA signaling in hypertrophied heart, Int. Heart J. 58 (1) (2017) 107–114.
[53] D. Lai, J. Gao, X. Bi, H. He, X. Shi, S. Weng, Y. Chen, Y. Yang, Y. Ye, G. Fu, Erratum to: the Rho kinase inhibitor, fasudil, ameliorates diabetes-induced cardiac dysfunction by improving calcium clearance and actin remodeling, J. Mol. Med. 95 (2) (2017) 167.
[54] D. Lai, J. Gao, X. Bi, H. He, X. Shi, S. Weng, Y. Chen, Y. Yang, Y. Ye, G. Fu, The Rho kinase inhibitor, fasudil, ameliorates diabetes-induced cardiac dysfunction by improving calcium clearance and actin remodeling, J. Mol. Med. 95 (2) (2017) 155–165.
[55] C. Mera, I. Godoy, R. Ramirez, J. Moya, M.P. Ocaranza, J.E. Jalil, Mechanisms of favorable effects of Rho kinase inhibition on myocardial remodeling and systolic function after experimental myocardial infarction in the rat, Ther. Adv. Cardiovasc. Dis. 10 (1) (2016) 4–20.
[56] T. Hattori, H. Shimokawa, M. Higashi, J. Hiroki, Y. Mukai, H. Tsutsui, K. Kaibuchi, A. Takeshita, Long-term inhibition of Rho-kinase suppresses left ventricular remodeling after myocardial infarction in mice, Circulation 109 (18) (2004) 2234–2239.
[57] L. Tan, N. Pan, L. Yu, R. Yu, B. Yang, The effects of Fasudil at different doses on acute myocardial infarction in rats, Acta Cardiol. Sin. 29 (6) (2013) 524–530.
[58] A. Phrommintikul, L. Tran, A. Kompa, B. Wang, A. Adrahtas, D. Cantwell, D.J. Kelly, H. Krum, Effects of a Rho kinase inhibitor on pressure overload induced cardiac hypertrophy and associated diastolic dysfunction, Am. J. Physiol. Heart Circ. Physiol. 294 (4) (2008) H1804–H1814.
[59] R. Guo, Y. Su, J. Yan, H. Sun, J. Wu, W. Liu, Y. Xu, Fasudil improves short-term echocardiographic parameters of diastolic function in patients with type 2 diabetes with preserved left ventricular ejection fraction: a pilot study, Heart Vessel. 30 (1) (2015) 89–97.
[60] X. Zhang, X. Zhang, S. Wang, J. Luo, Z. Zhao, C. Zheng, J. Shen, Effects of Fasudil on patients with pulmonary hypertension associated with left ventricular heart failure with preserved ejection fraction: a prospective intervention study, Can. Respir. J. 2018 (2018) 3148259.
[61] T. Shimizu, J.K. Liao, Rho kinases and cardiac remodeling, Circ. J. 80 (7) (2016) 1491–1498.
[62] I.M. Berenjeno, X.R. Bustelo, Identification of the Rock-dependent transcriptome in rodent fibroblasts, Clin. Transl. Oncol. 10 (11) (2008) 726–738.
[63] C.L. Lau, V.M. Perreau, M.J. Chen, H.S. Cate, D. Merlo, N.S. Cheung, R.D. O'Shea, P.M. Beart, Transcriptomic profiling of astrocytes treated with the rho kinase inhibitor fasudil reveals cytoskeletal and pro-survival responses, J. Cell. Physiol. 227 (3) (2012) 1199–1211.
[64] M. Boerma, Q. Fu, J. Wang, D.S. Loose, A. Bartolozzi, J.L. Ellis, S. McGonigle, E. Paradise, P. Sweetnam, L.M. Fink, M.C. Vozenin-Brotons, M. Hauer-Jensen, Comparative gene expression profiling in three primary human cell lines after treatment with a novel inhibitor of Rho kinase or atorvastatin, Blood Coagul. Fibrinol. 19 (7) (2008) 709–718.
[65] V. Wang, D.A. Davis, R. Yarchoan, Identification of functional hypoxia inducible factor response elements in the human lysyl oxidase gene promoter, Biochem. Biophys. Res. Commun. 490 (2) (2017) 480–485.
[66] S. Gao, J. Zhou, Y. Zhao, P. Toselli, W. Li, Hypoxia-response element (HRE)-directed transcriptional regulation of the rat lysyl oxidase gene in response to cobalt and cadmium, Toxicol. Sci. 132 (2) (2013) 379–389.
[67] N. Segond, S.A. Degrelle, S. Berndt, E. Clouqueur, C. Rouault, B. Saubamea, P. Dessen, K.S. Fong, K. Csiszar, J. Badet, D. Evain-Brion, T. Fournier, Transcriptome analysis of PPARgamma target genes reveals the involvement of lysyl oxidase in human placental cytotrophoblast invasion, PLoS One 8 (11) (2013) e79413.
[68] A. Sethi, W. Mao, R.J. Wordinger, A.F. Clark, Transforming growth factor-beta induces extracellular matrix protein cross-linking lysyl oxidase (LOX) genes in human trabecular meshwork cells, Invest. Ophthalmol. Vis. Sci. 52 (8) (2011) 5240–5250.
[69] S. Gao, Y. Zhao, L. Kong, P. Toselli, I.N. Chou, P. Stone, W. Li, Cloning and characterization of the rat lysyl oxidase gene promoter: identification of core promoter elements and functional nuclear factor I-binding sites, J. Biol. Chem. 282 (35) (2007) 25322–25337.
[70] S. Yokota, N. Chosa, S. Kyakumoto, H. Kimura, M. Ibi, M. Kamo, K. Satoh, A. Ishisaki, ROCK/actin/MRTF signaling promotes the fibrogenic phenotype of fibroblast-like synoviocytes derived from the temporomandibular joint, Int. J. Mol. Med. 39 (4) (2017) 799–808.
[71] E.M. Small, J.E. Thatcher, L.B. Sutherland, H. Kinoshita, R.D. Gerard, J.A. Richardson, J.M. Dimaio, H. Sadek, K. Kuwahara, E.N. Olson, Myocardin-related transcription factor-a controls myofibroblast activation and fibrosis in response to myocardial infarction, Circ. Res. 107 (2) (2010) 294–304.
[72] A.S. Narayanan, R.C. Siegel, G.R. Martin, On the inhibition of lysyl oxidase by -aminopropionitrile, Biochem. Biophys. Res. Commun. 46 (2) (1972) 745–751.
[73] S.T. Jung, M.S. Kim, J.Y. Seo, H.C. Kim, Y. Kim, Purification of enzymatically active human lysyl oxidase and lysyl oxidase-like protein from Escherichia coli inclusion bodies, Protein Expr. Purif. 31 (2) (2003) 240–246.
[74] E.C. El Hajj, M.C. El Hajj, V.K. Ninh, J.M. Bradley, M.A. Claudino, J.D. Gardner, Detrimental role of lysyl oxidase in cardiac remodeling, J. Mol. Cell. Cardiol. 109 (2017) 17–26.
[75] E.C. El Hajj, M.C. El Hajj, V.K. Ninh, J.D. Gardner, Cardioprotective effects of lysyl oxidase inhibition against volume overload-induced extracellular matrix remodeling, Exp. Biol. Med. 241 (5) (2016) 539–549.
[76] E. Martinez-Martinez, C. Rodriguez, M. Galan, M. Miana, R. Jurado-Lopez, M.V. Bartolome, M. Luaces, F. Islas, J. Martinez-Gonzalez, N. Lopez-Andres, V. Cachofeiro, The lysyl oxidase inhibitor (beta-aminopropionitrile) reduces leptin profibrotic effects and ameliorates cardiovascular remodeling in diet-induced obesity in rats, J. Mol. Cell. Cardiol. 92 (2016) 96–104.
[77] J. Gonzalez-Santamaria, M. Villalba, O. Busnadiego, M.M. Lopez-Olaneta, P. Sandoval, J. Snabel, M. Lopez-Cabrera, J.T. Erler, R. Hanemaaijer, E. Lara-Pezzi, F. Rodriguez-Pascual, Matrix cross-linking lysyl oxidases are induced in response to myocardial infarction and promote cardiac dysfunction, Cardiovasc. Res. 109 (1) (2016) 67–78.